Cell Reports

Article

The gut microbiota of environmentally enriched mice regulates visual cortical plasticity

Graphical abstract

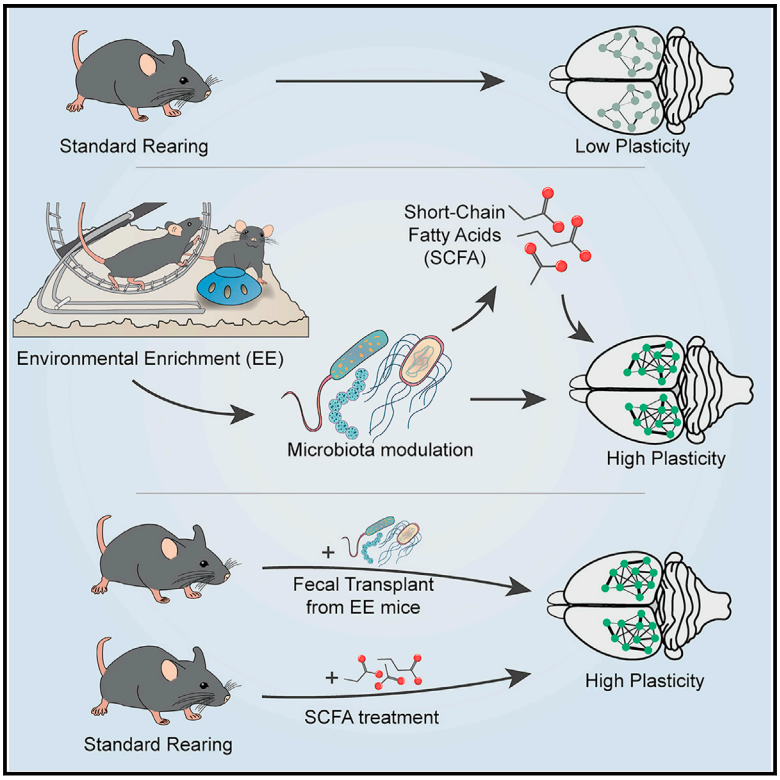

Highlights

- Housing mice in an enriched environment changes the gut microbiota
- An intact gut microbiota is necessary for enrichment-driven cortical plasticity
- Short-chain fatty acids modulate microglia morphology and visual cortical plasticity
- The pro-plasticity phenotype of enriched mice is transferred by fecal transplant

Authors

Leonardo Lupori, Sara Cornuti, Raffaele Mazziotti, ..., Giulia Sagona, Tommaso Pizzorusso, Paola Tognini

Correspondence

paola.tognini@unipi.it

In brief

Lupori et al. find that the gut microbiota is a key contributor to the effects of environmental enrichment on visual cortical plasticity. Depleting the microbiota of enriched mice blocks plasticity, while fecal microbiota transfer from enriched donors enhances plasticity in standard animals.

Lupori et al., 2022, Cell Reports *38*, 110212
January 11, 2022
https://doi.org/10.1016/j.celrep.2021.110212

CellPress

Cell Reports

CellPress
OPEN ACCESS

Article

The gut microbiota of environmentally enriched mice regulates visual cortical plasticity

Leonardo Lupori,[1,7] Sara Cornuti,[1,7] Raffaele Mazziotti,[2] Elisa Borghi,[3] Emerenziana Ottaviano,[3] Michele Dei Cas,[3] Giulia Sagona,[2] Tommaso Pizzorusso,[1,4,5,8] and Paola Tognini[1,6,8,9,*]

[1]BIO@SNS Lab, Scuola Normale Superiore, 56126 Pisa, Italy
[2]Department of Developmental Neuroscience, IRCCS Stella Maris Foundation, 56128 Pisa, Italy
[3]Department of Health Sciences, Università degli Studi di Milano, 20142 Milan, Italy
[4]Department of Neuroscience, Psychology, Drug Research and Child Health NEUROFARBA University of Florence, 50100 Florence, Italy
[5]Institute of Neuroscience, National Research Council, 56124 Pisa, Italy
[6]Department of Translational Research and New Technologies in Medicine and Surgery, University of Pisa, 56126 Pisa, Italy
[7]These authors contributed equally
[8]Senior author
[9]Lead contact
*Correspondence: paola.tognini@unipi.it
https://doi.org/10.1016/j.celrep.2021.110212

SUMMARY

Exposing animals to an enriched environment (EE) has dramatic effects on brain structure, function, and plasticity. The poorly known ''EE-derived signals'' mediating the EE effects are thought to be generated within the central nervous system. Here, we shift the focus to the body periphery, revealing that gut microbiota signals are crucial for EE-driven plasticity. Developmental analysis reveals striking differences in intestinal bacteria composition between EE and standard rearing (ST) mice, as well as enhanced levels of short-chain fatty acids (SCFA) in EE mice. Depleting the microbiota of EE mice with antibiotics strongly decreases SCFA and prevents activation of adult ocular dominance plasticity, spine dynamics, and microglia rearrangement. SCFA treatment in ST mice mimics EE induction of ocular dominance plasticity and microglial remodeling. Remarkably, transferring the microbiota of EE mice to ST recipients activates adult ocular dominance plasticity. Thus, experience-dependent changes in gut microbiota regulate brain plasticity.

INTRODUCTION

The complexity of brain circuits is sculpted both by innate genetic programs and environmental stimuli capable of activating brain plasticity and, in turn, reshaping brain circuits and behavior. This process is particularly evident in the development and refinement of neuronal circuits belonging to sensory modalities (Hübener and Bonhoeffer, 2014). Since the 1960s, scientists noticed that raising rodents in an enriched housing condition characterized by elevated social interactions, and cognitive, sensory, and motor stimulations (Kempermann, 2019) could improve their learning and memory abilities (Rosenzweig and Bennett, 1996). Interestingly, the benefits of this enriched environment (EE) go beyond memory features and embrace several aspects of brain functionalities, including healthy development, emotional behavior, recovery from neural damage, and positive effects on a variety of preclinical models of neuropsychiatric diseases (Nithianantharajah and Hannan, 2006). Indeed, EE is known to enhance neuronal activation, signaling, and plasticity throughout various brain regions, including sensory areas, and at different ages (Baroncelli et al., 2010). For example, ocular dominance plasticity, a change in eye preference of cortical cell responses induced by monocular deprivation (MD), is typically observed during a critical period of postnatal development (Hensch, 2005; Levelt and Hübener, 2012). However, EE mice showed strong ocular dominance plasticity (Greifzu et al., 2014) and recovery from amblyopia also during adulthood (Sale et al., 2007; Tognini et al., 2012). Moreover, EE was found to accelerate several molecular and functional aspects of visual cortical development (Cancedda et al., 2004), indicating that the visual system is highly influenced by EE both during development and adulthood.

A variety of mechanisms have been discovered to contribute to the EE plasticity enhancement, such as increased hippocampal neurogenesis, changes in the excitatory/inhibitory circuit ratio, promotion of structural plasticity of dendritic spines, alteration in BDNF levels, microglia rearrangement, chromatin remodeling, and others (Baroncelli et al., 2010; Kempermann, 2019; Pizzorusso et al., 2007). So far, all the mechanisms explaining EE influence on neural plasticity have been searched inside the brain. However, the complexity of EE stimuli should bring benefits to the whole body. Thus, we seek to investigate if signals coming from the periphery could participate in EE-driven plasticity in the central nervous system, focusing on the gut microbiota.

The intestinal microbiota has emerged as a complex regulator of system-wide physiology (Schroeder and Bäckhed, 2016).

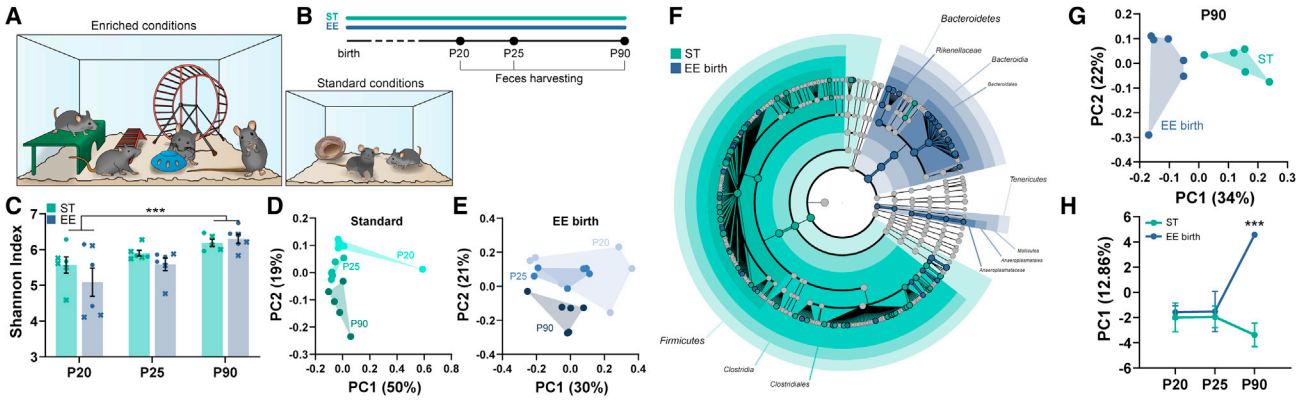

Figure 1. EE modulates the gut microbiota composition

(A) Schematic of enriched and standard housing conditions.

(B) Experimental timeline.

(C) Shannon Index for all the conditions, showing alpha-diversity (n = 6 EE [three males and three females], n = 6 ST [four males, two females], n = 5 in P90 ST [three males and two females], two-way ANOVA, age*housing, age, $F_{2,29}$ = 8.764 p = 0.0011, post hoc Tukey test P20 versus P90 p < 0.001; crosses represent males and circles represent females).

(D and E) PCoA showing beta-diversity (unweighted UniFrac distance) at different ages in ST and EE birth animals (ANOSIM test, ST group: P20 versus P25 R = 0.32 p = 0.002, P25 versus P90 R = 0.424 p = 0.004, P20 versus P90 R = 0.461 p = 0.009; EE group: P20 versus P25 R = −0.007 p = 0.46, P25 versus P90 R = 0.483 p = 0.0015, P20 versus P90 R = 0.291 p = 0.008).

(F) Cladogram of differential bacterial composition (ST versus EE, P90) using LEfSe analysis. Shaded areas represent taxa significantly enriched in one of the conditions.

(G) PCoA between ST and EE birth animals at P90 (ANOSIM test, ST versus EE birth, P90: R = 0.445 p = 0.0015).

(H) First principal component from an integrated PCA of OTU abundance of all the experimental groups (two-way ANOVA time*housing, interaction $F_{2,28}$ = 8.482 p = 0.0013, post hoc Holm-Sidak ST versus EE birth (P90) t_{28} = 5.18 p < 0.001).

Data in (C) and (H) are presented as mean ± SEM.

Classically, gut microbes have been studied in the context of host metabolic homeostasis and immune system development and function (Nicholson et al., 2012; Rooks and Garrett, 2016; Tremaroli and Bäckhed, 2012). Nevertheless, the relationship between the intestinal microbiota and its host seems to be deeply intricate, going far beyond the influence on metabolism and immunity (Murakami and Tognini, 2019). Indeed, recent reports have suggested the commensals to play an important role in brain-related processes: myelination (Gacias et al., 2016; Hoban et al., 2016), microglia maturation (Erny et al., 2015), neurogenesis (Möhle et al., 2016), blood-brain-barrier permeability (Braniste et al., 2014), and finally influence on behavioral outcomes (Boehme et al., 2021; Cowan et al., 2020; Forsythe and Bienenstock, 2016; Hsiao et al., 2013; Tognini, 2017) and neural plasticity (Darch et al., 2021; Buffington et al., 2016, 2021). Despite this evidence, little is known about how intestinal bacteria impinge on neuronal function and, especially, if there is a link between experience-dependent plasticity and the gut microbiota. In this study, we show that EE significantly alters the intestinal microbiota in C57BL/6J mice, and that microbiota manipulation through antibiotics interferes with EE-driven visual cortical plasticity, dendritic spine dynamics, and microglial rearrangement. Strikingly, the fecal microbiota transplant (FT) from EE donors to adult standard (ST) mice was able to enhance ocular dominance plasticity in the ST recipients. Overall, our study introduces a key concept: environment-dependent changes in the gut microbiota composition can regulate brain plasticity.

RESULTS

EE modulates the composition of the gut microbiota

C57BL/6J mice were reared from birth in ST (standard laboratory cage, containing only bedding and nesting material), or EE conditions (large cage, containing also running wheels, and differently shaped toys; Figure 1A) from birth (EE birth). In order to investigate the intestinal bacteria composition, fresh feces were collected in a longitudinal way from ST and EE birth mice before weaning: postnatal day (P) 20, a few days after weaning (P25), and during adulthood (P90) (Figure 1B). The bacterial DNA was extracted from the feces and analyzed through 16S rRNA sequencing (seq) (bacterial abundance is reported in Tables S1 and S2).

To analyze the results, we first calculated alpha-diversity, a parameter reflecting species richness in a microbial ecosystem (Thukral, 2017). We observed that there was a significant increase in alpha-diversity in both ST and EE mice between P20 and P90 (Figures 1C and S1A); however, there were no intergroup differences at any age tested, indicating that housing animals in EE did not alter the alpha-diversity in the microbial ecosystem. Second, we computed beta-diversity, which measures the degree of phylogenetic similarity between microbial communities, using the unweighted UniFrac algorithm (Lozupone and Knight, 2005). Principal coordinate analysis (PCoA) of unweighted UniFrac distance showed that the microbiota of ST animals clustered in different groups at P20, P25, and P90 (Figure 1D). EE birth mice also displayed an age-dependent

difference between P90 and P20 or P25 mice, although P20 and P25 were not significantly different (Figure 1E).

Third, we sought to explore differences in the bacterial composition between EE birth and ST conditions by using linear discriminant analysis (LDA) effect size (LEfSe) method (Segata et al., 2011). LEfSe revealed a relatively small, although significant difference in some taxa in P20 ST mice versus P20 EE, as shown by the cladogram in Figure S1B, and by the LDA score in Figure S1C. In particular, at P20 species in Mollicutes class, Anearoplasmataceae family and Anearoplasmatales order were significantly more abundant in EE with respect to ST. PCoA of the unweighted UniFrac distance matrix confirmed the phylogenetic similarities between ST and EE at P20 (Figure S1D). At P25, the cladogram displayed a situation similar to P20, in addition taxa in the Erysipelotrichia class, Erysipelotrichales order, and Erysipelotrichaceae family were more abundant in EE than in ST mice (Figures S2A and S2B). Also, beta-diversity showed clustering in more separate groups (Figure S2C). Intriguingly, at P90 the composition of the microbiota in EE birth mice dramatically diverged from that of age-matched ST rodents, as displayed by the cladogram in Figure 1F. The enrichment in taxa belonging to Tenericutes already present at P20 and P25 was maintained. Furthermore, species present in the family Rikenellaceae, the order Bacteroidales and the class Bacteroidia, all included in the phylum Bacteroidetes, were more abundant in EE. On the other hand, several taxa belonging to the phylum Firmicutes were significantly enriched in ST (Figure 1F, Figure S3). As expected, PCoA of beta-diversity calculated through the unweighted UniFrac distance demonstrated that EE and ST microbes clustered in separate groups at P90 (Figure 1G), indicating robust differences in the membership of gut bacteria between EE and ST mice.

Principal component analysis (PCA) of operational taxonomic units (OTU) abundance comparing ST and EE birth mice at all ages and considering the first component (PC1) indicated that the differences in the microbiota composition were significant only at P90, while higher similarity was present in microbe composition at P20 and P25 (Figure 1H).

Thus, our 16S rRNA-seq data demonstrated a progressive developmental divergence of the microbiota composition between mice living in EE and ST conditions. Considering that EE is able to promote different forms of plasticity in a variety of brain areas during adulthood, we further explored the possible link between gut microbiota and EE-driven plasticity in the adult visual cortex.

Depletion of the gut microbiota in EE mice prevented ocular dominance plasticity

Short periods of MD do not induce ocular dominance plasticity in adult ST mice (Lehmann and Löwel, 2008), whereas they induce strong plasticity in adult EE mice, demonstrating that EE potently activates visual cortical plasticity (Greifzu et al., 2014; Sale et al., 2007). To investigate the contribution of signals coming from the intestinal microbes on EE-induced visual cortical plasticity, the microbiota of the animals living in EE was depleted using a wide-spectrum antibiotic cocktail (ABX: ampicillin, neomycin, metronidazole, and vancomycin) in drinking water. The ABX treatment started 1 week before birth (ABX in dams' water) and continued until P120 (Figure 2A). The efficacy of the treatment was demonstrated by 16S rRNA-seq of fecal bacteria after ABX administration (Figures S4A and S4B). In order to test ocular dominance plasticity, mice were subjected to optical imaging of the intrinsic optical signal (IOS, Figures 2B–2D). IOS was performed before and after 3 days of MD (3dMD) in the same subjects (Figure 2A). Strikingly, ABX treatment completely prevented ocular dominance plasticity in adult EE mice (Figures 2E and 2F). As a control, we also confirmed that 3dMD elicited an ocular dominance shift in ST mice during the critical period, but not in adult mice (Figures S4C and S4D). Overall, these data indicate that an intact intestinal microbiota is necessary for the enhancement of adult plasticity observed in EE rodents.

To rule out any developmental effects of the ABX treatment from birth, we performed the 3dMD experiment in mice reared in EE and treated with ABX for only 5 weeks from P85 until P120 (Figure 2G). This short EE protocol during adulthood was sufficient to induce ocular dominance plasticity in response to 3dMD (Figures 2H and 2I, EE group). The induction of ocular dominance plasticity by brief EE was also sensitive to microbiota depletion. Indeed, if ABX was administered simultaneously to EE, the EE-driven plasticity was blocked (Figures 2H and 2I, EE + ABX group). As metronidazole could cross the blood-brain-barrier (Champagne-Jorgensen et al., 2019), an ABX devoid of metronidazole (only ampicillin, vancomycin, and neomycin) was tested in adult EE mice. The new antibiotic cocktail was able to prevent visual cortical plasticity as the ABX (Figure S4E). Conversely, the treatment with metronidazole alone for 5 weeks simultaneously to EE did not block the EE-driven enhancement of ocular dominance plasticity in adult mice (Figure S4E), suggesting that the specific antimicrobial effects of metronidazole are not sufficient to counteract the EE enhancement in plasticity, and ruling out a direct action of metronidazole on cortical neurons.

Importantly, before 3dMD, visual responses and baseline ocular dominance of both EE + ABX-birth and EE + ABX mice were not different from their controls (Figures S4F and S4G), thus excluding a possible direct effect of ABX treatment on cortical responses.

In conclusion, an unperturbed intestinal microbiota is necessary for EE promotion of ocular dominance plasticity.

EE effects on dendritic spines and microglia morphology are blocked by ABX administration

Dendritic spines are protrusions harboring the postsynaptic machinery of excitatory synapses. Spines are dynamic compartments, and their structural remodeling is thought to be one of the signatures of the ongoing rewiring of neuronal circuits (Holtmaat and Svoboda, 2009). Since EE is known to increase the density and dynamics of dendritic spines in the cortex (Ali et al., 2019; Xu et al., 2016), we asked whether manipulating the gut microbiota could interfere with EE-driven plasticity through mechanisms involving spines remodeling. We performed repeated two-photon *in vivo* imaging to analyze dendritic spines in a cohort of transgenic Thy1-GFP-M mice expressing GFP in a sparse population of layer V pyramidal neurons in the visual cortex (Feng et al., 2000; Jung and Herms, 2014). We acquired images of the same apical dendritic segments for 40 days in

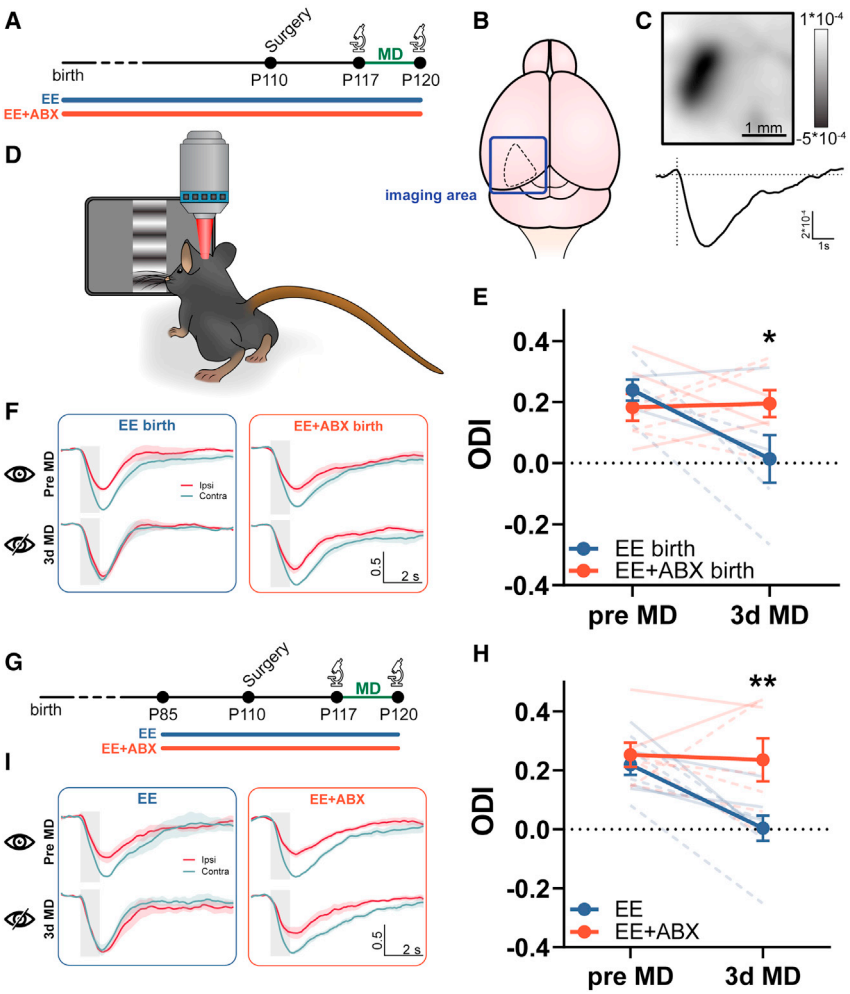

Figure 2. ABX treatment prevents the plasticity enhancing effect of EE

(A) Experimental timeline.

(B and D) Schematic of the imaging setup and imaging area.

(C) Representative intrinsic signal response (top: response image, bottom: signal timeline) from the binocular primary visual cortex to visual stimulation. Scale bar, 1 mm.

(E) Ocular Dominance Index (ODI) before and after MD. Thin lines represent single animals (n = 6 [two males and four females] EE birth, n = 7 [three males and four females] EE + ABX-birth, two-way RM ANOVA time*housing, interaction $F_{1,11}$ = 6.716 p = 0.025, post hoc Holm-Sidak, EE birth versus EE + ABX-birth (3dMD) t_{11} = 3.3 p = 0.013).

(F) Normalized response timeline to contralateral (contra) and ipsilateral (ipsi) eye stimulation before and after MD for both groups. Shaded area represents visual stimulus duration.

(G) Experimental timeline.

(H) ODI before and after MD (n = 8 EE (four males, four females), n = 7 EE + ABX (two males, five females), two-way RM ANOVA time*housing, interaction $F_{1,13}$ = 5.936 p = 0.030, post hoc Holm-Sidak, EE versus EE + ABX (3dMD) t_{26} = 3.342 p = 0.0051).

(I) Normalized response timeline to contralateral (contra) and ipsilateral (ipsi) eye stimulation before and after MD for both groups. Shaded area represents visual stimulus duration. In (E) and (H), solid lines represent males and dashed lines represent females.

Data in (E), (F), (H), and (I) are presented as mean ± SEM.

the visual cortex (Figure 3A). After two baseline imaging time points (1-day interval), animals were put in EE cages for 35 days (5 weeks) and received ABX in drinking water (EE + ABX group) or regular water (EE group) (Figure 3B). The same dendritic segments were imaged in the two groups 9, 10, 19, 20, 34, and 35 days after the beginning of EE (Figures 3B–3D).

The analysis of spine density revealed a significant interaction between time and housing conditions. Post hoc tests showed that spine density in EE mice was significantly larger than in EE + ABX mice at all times after EE start, but it did not differ at baseline. Comparing spine density within each group at different time points confirmed that spine density did not change over time in the EE + ABX group. By contrast, the EE group displayed a dramatic increase in spine density occurring between the baseline and the first imaging time point after the beginning of EE (10 days after EE start, Figures 3E and 3F). This observation was confirmed by analyzing the data from single animals. Indeed, animals in the EE group showed a significant 25% increase in spine density after 10 days of EE with respect to baseline levels, while this effect was prevented in animals treated with ABX (Figure 3H). To further dissect this effect, we calculated spine formation and elimination rates during this critical time window (Figures 3G and S5A). Across the first 10 days of EE, spine elimination rates were not different between the two groups; however, animals treated with ABX had a remarkably lower spine formation rate compared with controls, thus explaining the lack of increase in spine density in the ABX-treated group (Figure 3I). Moreover, the EE + ABX group had a significantly lower spine formation rate with respect to EE controls, also analyzing the short-term 24-h spine dynamics. Indeed, short-term formation rate was comparable between the two groups at baseline, but significantly differed after 10 days of EE. Conversely, elimination rates were similar between the two groups (Figure. 3I). These data suggest that the ABX treatment prevents the increase in spine density typical of enriched animals by interfering with the process of formation of new spines and not by destabilizing existing spines or increasing the opposing process of spine elimination. This interpretation is further corroborated by the analysis of dendritic spine survival curves. Indeed, both for the subset of spines originally present at the first time point and for the subset of newborn spines that appeared after the start of EE, the treatment with ABX did not have any effect on survival curves (Figure S5B).

Ocular dominance plasticity and activity-dependent regulation of dendritic spines during the critical period of the visual cortex involve microglial cells (Cheadle et al., 2020; Sipe et al., 2016). Previous reports demonstrated that EE housing resulted in

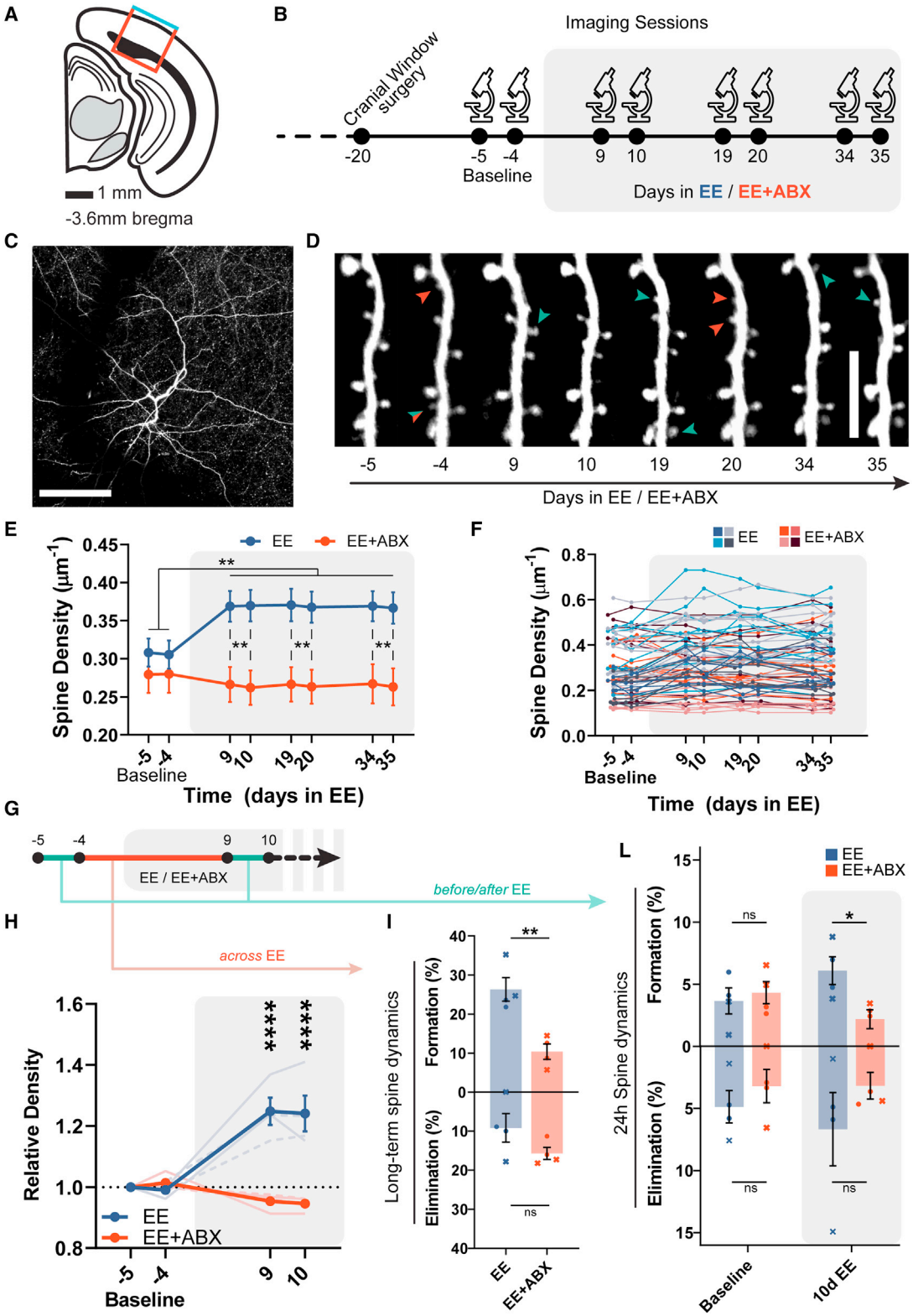

Figure 3. ABX treatment modulates the effect of EE on dendritic spines

(A) Schematic coronal section of the primary visual cortex showing the imaging site.

(B) Experimental timeline.

(legend continued on next page)

more numerous and longer microglial processes in different brain regions (Ali et al., 2019; Xu et al., 2016). Thus we asked whether prevention of EE effects by ABX treatment could also be associated with altered microglial morphology. To answer this question, we performed immunofluorescence for IBA-1, a specific microglial marker, in fixed sections of the visual cortex of three experimental groups: adult mice housed in EE for 5 weeks receiving ABX in drinking water or drinking regular water, and age-matched ST animals. Quantitative three-dimensional morphometric analysis of microglia highlighted striking differences between ST- and EE-housed mice (Figure 4A). Using Sholl analysis, which reflects microglial process arborization, we found a robust and significant increase in microglia complexity in the EE mice compared with the ST group (Figure 4B). This difference was particularly compelling at a distance of 14 to 50 μm from the soma (See Table S3). Importantly, the ABX treatment completely prevented the effect of EE on microglia, maintaining the complexity to the levels of the ST group (Figures 4A and 4B).

To further explore the morphological changes, we examined single features of microglia ramification. We observed significantly shorter processes, and a significant decrease in the number of branching points and terminal points in mice housed in EE and subjected to ABX treatment compared with animals in EE condition alone, while ST animals displayed parameters very similar to EE + ABX (Figures 4C–4E and S5C–S5E).

Overall, these data indicate that ABX treatment dramatically affects the microglial morphology of EE mice.

Short-chain fatty acid administration enhances ocular dominance plasticity in adult mice and affects microglia morphology

To dissect the possible mechanisms through which the gut microbiota of EE mice could promote cortical plasticity in adulthood, we focused on commensal-derived metabolites. Short-chain fatty acids (SCFAs), the main metabolites produced in the colon by bacterial fermentation of dietary fibers and resistant starch, have been shown to play a key role in neuro-immuno-endocrine regulation, and in several aspects of the gut-microbiota-brain axis (Dalile et al., 2019). Gas chromatography coupled with flame ionization detector (GC-FID) analysis of fecal-derived SCFA showed a significant increase in EE with respect to ST mice in acetate, propionate, and butyrate concentration, whereas ABX administration completely blocked this effect (Figures S6A–S6C). Based on these results, we explored the possibility that SCFA could be microbiota-derived metabolites mediating the pro-plasticity effect of EE. An SCFA mix, containing butyrate, propionate, and acetate, was dissolved in the drinking water and administered to ST adult mice for 4 weeks. During the last week of treatment, mice were subjected to IOS imaging before and after 3dMD (Figure 5A). Strikingly, SCFA in drinking water was able to promote visual cortical plasticity in adult ST mice, while, as expected, control age-matched ST animals drinking regular water did not show the ocular dominance shift (Figures 5B and 5C). Importantly, SCFA administration also altered the morphology of microglial cells in the visual cortex mimicking EE effects (Figure 5D). Indeed, SCFA treatment significantly increased process arborization (Figure 5E and Table S4 for Sidak's multiple comparisons test), filament length, and the number of branching points and terminal points in SCFA-treated mice with respect to ST controls (Figures 5F–5H, S6D–S6F).

Our results suggest that SCFAs could be candidate molecules through which the microbiota influence cortical plasticity, possibly involving microglia remodeling mechanisms.

Fecal transplantation transfers the plastic phenotype from EE to ST adult mice

To provide further independent evidence to support the role of intestinal microbes in ocular dominance plasticity of EE mice, adult ST mice were subjected to an FT experiment. Fresh feces from EE mice or ST animals as a control were collected and a PBS suspension was freshly prepared. The FT was performed in conventionally raised ST recipient mice, previously treated with ABX to favor the engraftment of the new species (Figure 6A). FT mice were subjected to oral gavage with the donor feces suspension for 5 days. To exclude a direct effect of the ABX pretreatment on plasticity, a further control group of mice was administered with PBS (the vehicle of the donor feces suspension). After 4 weeks, ocular dominance plasticity was investigated through IOS imaging (Figure 6A). Remarkably, transferring feces from EE donors to ST recipients was able to induce visual cortical plasticity in ST mice, while, as expected, control animals inoculated with feces from ST donor mice or the PBS vehicle did not display any ocular dominance shift after 3dMD (Figures 6B and 6C).

(C) Representative low magnification image of a neuron. Scale bar, 100 μm.
(D) Representative high-magnification images of a dendritic segment at eight consecutive time points. Green arrowheads: spine formation, red arrowheads: spine elimination. Scale bar, 10 μm.
(E and F) Spine density over time. Averages per dendrites (E) and single dendrites (F), color coded for the animals to which they belong (n = 39 EE, n = 28 EE + ABX, two-way RM ANOVA time*treatment, interaction $F_{7,455} = 20.97$ $p < 0.0001$, post hoc Holm-Sidak, EE versus EE + ABX (9d-35d) $t_{54\text{-}61} > 3.15$ $p < 0.01$ for all comparisons; EE(9d-35d) versus EE(baseline) $t_{38} > 5.73$ $p < 0.0001$ for all comparisons.
(G) Schematic of the analysis for spine dynamics in (I) and (L).
(H) Spine density relative to the first imaging time point. Thin lines represent single animals (n = 4 EE (two males, two females), n = 4 EE + Abx (two males, two females), two-way RM ANOVA time*treatment, interaction $F_{3,18} = 28.60$ $p < 0.0001$, post hoc Holm-Sidak, EE versus EE + Abx (9d-10d) $t_{24} > 7.52$ $p < 0.0001$ for al comparisons; EE(9d-10d) versus EE(-4) $t_{18} > 7.56$ $p < 0.0001$ for all comparisons).
(I) Long-term (10d) spine dynamics across the beginning of EE (n = 4 EE (two males, two females), n = 4 EE + ABX (two males, two females), Formation: unpaired two-tailed t test $t_6 = 4.42$ $p = 0.0045$; Elimination: unpaired 2-tailed t test $t_6 = 1.65$ $p = 0.15$) (L) Short-term 24-h spine dynamics before and after EE. (n = 4 EE (two males, two females), n = 4 EE + ABX (two males, two females). Formation: two-way RM ANOVA time*treatment, interaction $F_{1,6} = 6.620$ $p = 0.042$, post hoc Holm-Sidak EE versus EE + ABX (10dEE) $t_{12} = 2.87$ $p = 0.028$; Elimination: two-way RM ANOVA time*treatment, no significant differences). In (I) and (L), crosses represent males and circles represent females; in (H), solid lines represent males and dashed lines represent females.
Data in (E), (H–L) are presented as mean ± SEM.

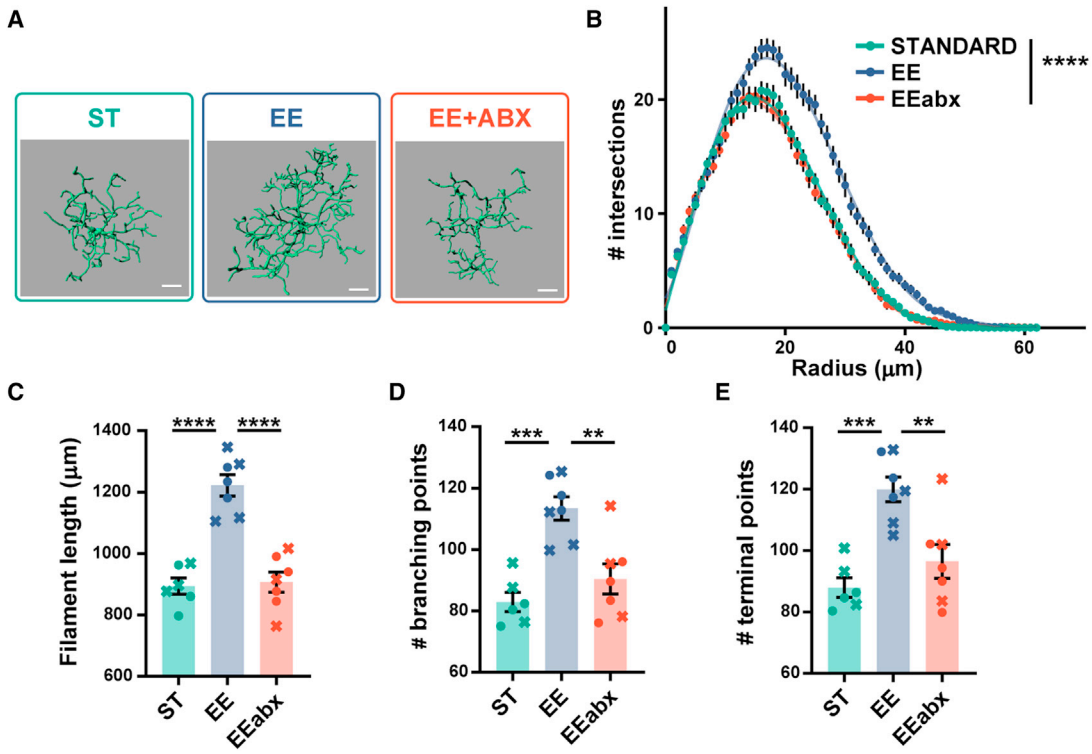

Figure 4. ABX treatment alters microglia morphology in EE mice

(A) IMARIS semi-automatic three-dimensional reconstruction and quantitative morphometric analysis of IBA-1+ microglia. Scale bar, 10 μm.

(B) Sholl analysis of microglial cells (n = 35 EE, n = 38 EE + ABX, n = 32 ST two-way ANOVA distance*treatment, interaction $F_{124,6324} = 6.284$, $p < 0.0001$, see Table S3 for Tukey's post hoc comparisons.

(C) Filaments length (Ordinary one-way ANOVA, $F_{2,17} = 34.19$ $p < 0.0001$, Tukey's post hoc ST versus EE $p < 0.0001$, EE versus EE + ABX $p < 0.0001$).

(D) Number of branching points (Ordinary one-way ANOVA, $F_{2,17} = 14.85$ $p = 0.0002$, Tukey's post hoc ST versus EE $p = 0.0002$, EE versus EE + ABX $p = 0.0023$).

(E) Number of terminals (Ordinary one-way ANOVA, $F_{2,17} = 13.79$ $p = 0.0003$, Tukey's post hoc ST versus EE $p = 0.0003$, EE versus EE + ABX $p = 0.0038$). (C–E) n = 7 EE (four males, three females), n = 7 EE + ABX (three males, four females), n = 6 ST (three males, three females); each symbol represents one mouse, crosses represent males and circles represent females. At least five cells measured per mouse.

Data in (B–E) are presented as mean ± SEM.

Importantly, PCoA of unweighted UniFrac distance showed that the microbiota of ST recipients after the FT with EE feces (postFT-EE) was overlapping the microbiota of EE donor mice, while the microbiota of ST animals before FT (preFT-EE) clustered in a separate group with respect to EE donors and postft (Figure 6D). Although still significantly different, the analysis of similarities (ANOSIM) R was only 0.17 in the EE donors versus postFT-EE comparison, indicating the presence of a substantial overlap in the phylogenetic composition of ST recipient and EE donor microbiota (Figure 6D, Table S5 for the relative bacteria abundance). No intergroup differences among preFT-EE, postFT-EE, and EE donors in microbial alpha-diversity were found (Figures S7A and S7B).

Altogether, those data demonstrate the efficacy of our FT protocol, and indicate that the "plastic phenotype" of the adult EE mouse can be transferred to an ST animal through the fecal microbiota.

DISCUSSION

Since the pioneering studies of Rosenzweig and his collaborators, EE has been widely used as a model for studies on experience-dependent regulation of brain function. Those studies demonstrated that EE dramatically affects brain morphology, chemistry, and physiology; eliciting remarkable plastic responses ranging from molecular to anatomic and functional changes (Rosenzweig and Bennett, 1996). Several investigations continued this line of research trying to understand the specific mechanisms through which EE affects brain plasticity to realize the EE translational potential. However, the mechanisms to explain the EE impact on brain circuits and behavior have been classically explored into the brain itself: among many others, studies identified changes in neurotrophin levels (Pham et al., 2002), altered expression of plasticity-related genes (Rampon et al., 2000) and synaptic proteins (Nithianantharajah et al., 2004; Song et al., 2018), inhibitory circuits remodeling, perineuronal net modifications (Sale et al., 2007; Slaker et al., 2016), and epigenetic mark changes (Fischer et al., 2007; Wang et al., 2013). Our study shifts the focus from the central nervous system to the periphery, revealing that signals coming from the gut microbiota contribute to EE-driven cortical plasticity (Figure 7).

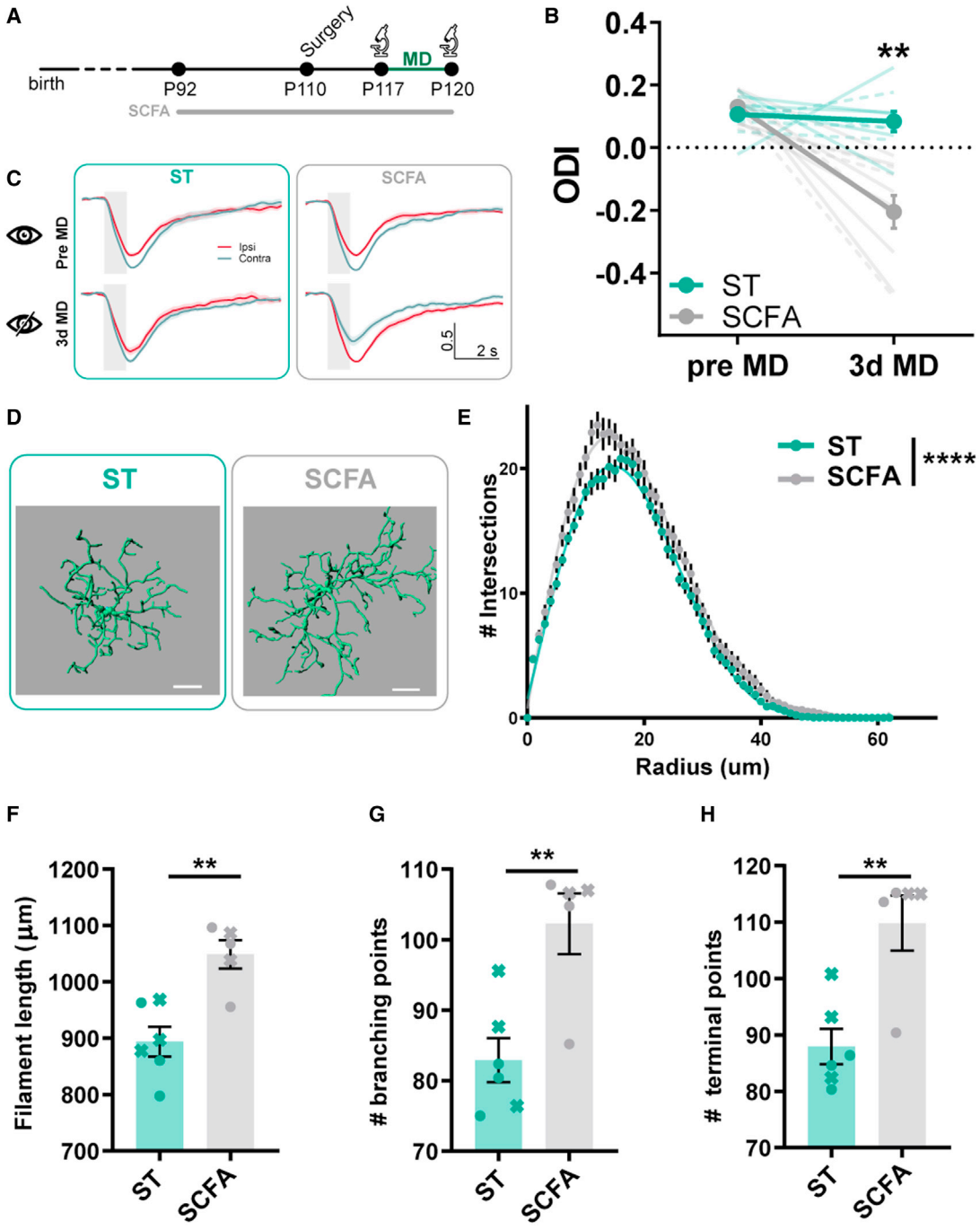

Figure 5. SCFA administration mimics the effect of EE on plasticity and microglia morphology

(A) Experimental timeline.

(B) ODI before and after MD. Thin lines represent single animals (n = 9 ST (five males, four females), n = 10 SCFA (six males, four females), two-way RM ANOVA time*treatment, interaction $F_{1,17} = 15.28$ p = 0.0011, post hoc Holm-Sidak, ST versus SCFA (3dMD) $t_{34} = 5.94$ p < 0.001). Solid lines represent males and dashed lines represent females.

(C) Normalized response timeline to contralateral (contra) and ipsilateral (ipsi) eye stimulation before and after MD for both groups. Shaded area represents visual stimulus duration.

(D) IMARIS semi-automatic three-dimensional reconstruction and quantitative morphometric analysis of IBA-1+ microglia. Scale bar, 10 µm.

(E) Sholl analysis of microglial cells (n = 32 ST, n = 25 SCFA, two-way ANOVA distance*treatment, interaction $F_{62,3410} = 1.903$, p < 0.0001, see Table S4 for Sidak's post hoc comparisons).

(F) Filaments length (unpaired two-tailed t test, $t_9 = 4.166$ p = 0.0024).

(legend continued on next page)

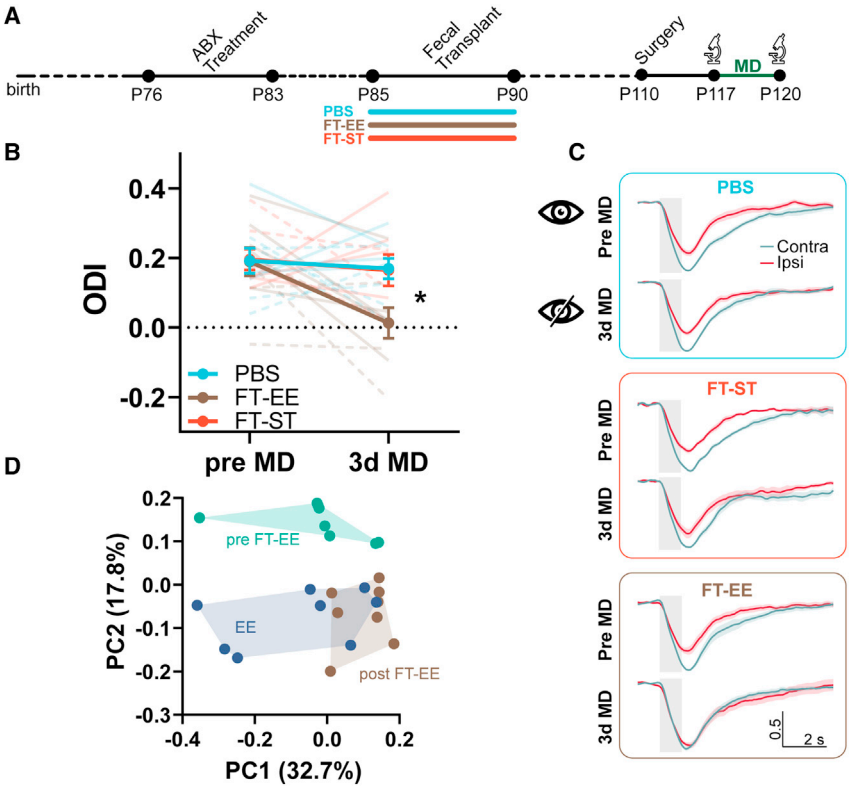

Figure 6. Fecal transplant ODI

(A) Experimental timeline.

(B) ODI before and after MD. Thin lines represent single animals (n = 9 PBS (four males, five females), n = 9 FT-EE (five males, four females), n = 8 FT-ST (five males, three females), two-way RM ANOVA time*treatment, interaction $F_{2,23}$ = 2.888 p = 0.076, post hoc Holm-Sidak, PBS versus FT-EE (3dMD) t_{46} = 2.92 p = 0.029); PBS versus FT-ST (3dMD) t_{46} = 0.094 p > 0.99; FT-EE versus FT-ST (3dMD) t_{46} = 2.773 p = 0.039.

(C) Normalized response timeline to contralateral (contra) and ipsilateral (ipsi) eye stimulation before and after MD for all groups. Shaded gray area represents visual stimulus duration.

(D) PCoA (unweighted UniFrac distance) of EE, preFT-EE and postFT-EE animals (n = 8 per group, ANOSIM test, preFT-EE versus EE, R = 0.32, p = 0.003; preFT-EE versus postFT-EE, R = 0.40, p = 0.001; EE versus postFT-EE R = 0.17, p = 0.03). In (B), solid lines represent males and dashed lines represent females.

Data in (B) and (C) are presented as mean ± SEM.

The gut microbiota is modulated by EE

Our study identifies two powerful regulators of the mouse gut microbiota: age and environment. Indeed, we found that fecal bacterial diversity (microbiota alpha-diversity) increases between P20 and P90 in both EE and ST mice. This increase in the complexity of the ecosystem was a general feature process of gut microbiota maturation, not linked to the rearing environment. Significant differences in the phylogenetic composition (beta-diversity) of the bacteria community at distinct ages were observed in ST and EE animals. Notably, EE dramatically altered the fecal microbiota composition. Importantly, this regulation is specific to EE and it is independent from the dietary regimen or other rearing conditions since the ST and EE cages were housed one next to the other and mice received the same food. The number of species differing between ST and EE mice was relatively small, but still significant, before and a few days after weaning. In particular, the LEfSe analysis at P20 revealed that species in the Mollicutes class, Anearoplasmataceae family, and Anearoplasmatales order were significantly more abundant in EE with respect to ST. At P25, species belonging to the same taxa were still significantly high in EE with respect to ST, in addition to species in the Erysipelotrichia class. However, the most striking difference was present in adulthood, when species belonging to the phyla Tenericutes and Bacteroidetes were significantly enriched in EE. Why the effect of EE was so prominent in adulthood, while at juvenile ages the species distinction was lower, has not been explored yet. We could speculate that this developmental regulation of EE effect on microbiota might be caused by the fact that adult animals could fully experience the complexity of the stimulation offered by EE. The gut microbiota could be particularly sensitive to features of the EE including physical activity, exploring new toys, spatial patterns of objects, which are activities preferred by older than little mice. However, we cannot exclude other microbiota remodelers starting to impinge on its composition during early postnatal development. For instance, differences in maternal care from enriched dams might account for the distinct composition observed before weaning. Also, the immune system of EE mice could be influenced to send specific signals to the intestinal microbes by still unknown stimuli, thus shaping the ecosystem toward a precise composition. Finally, as metabolism and the microbiota are deeply intertwined, metabolic cues might also play a role. For instance, physical exercise is an important EE component capable of modulating brain plasticity (van Praag et al., 2000); however, it cannot explain the full ocular dominance plasticity enhancement observed in EE rodents (Baroncelli et al., 2012). Some studies demonstrated changes in the microbiota composition and diversity of rodents after physical exercise, and an increase in the Bacteroidetes phylum and the Lachnospiraceae family (Evans et al., 2014; Mika et al., 2015), and recently EE has been shown to modulate the gut microbiota composition in adult rats (Higarza et al., 2021). Changes in bacteria families after diet or physical exercise were also correlated to behavioral alterations. For instance, increases in taxa

(G) Number of branching points (unpaired two-tailed t test, t_9 = 3.722 p = 0.0048).

(H) Number of terminals (unpaired two-tailed t test, t_9 = 3.911 p = 0.0036). (F–H) n = 6 ST (three males, three females), n = 5 SCFA (two males, three females), each symbol represents one mouse, crosses represent males and circles represent females. At least five cells measured per mouse.

Data in (B), (C), (E–H) are presented as mean ± SEM.

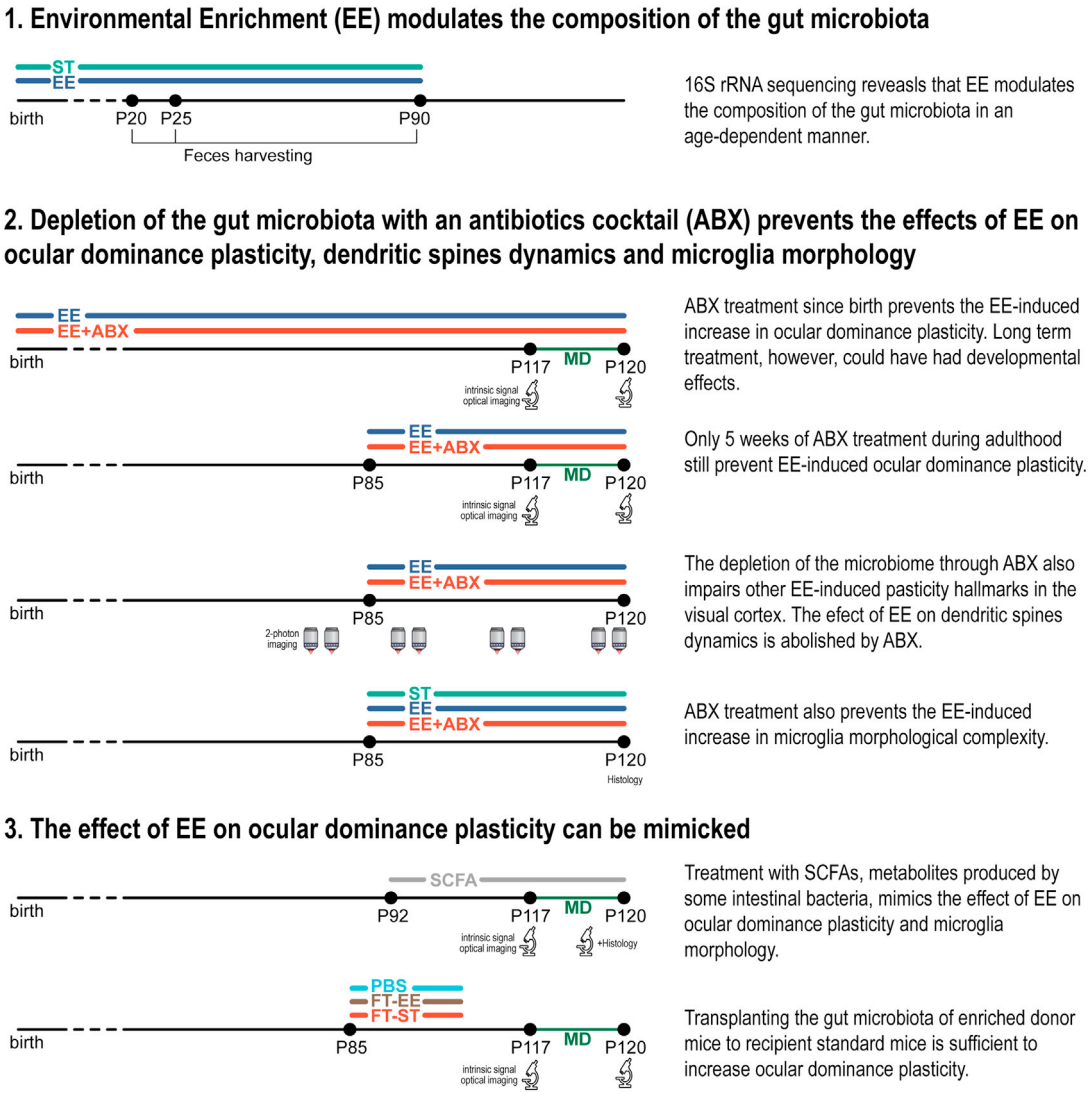

Figure 7. Results summary

Schematic overview of the experiments performed and the major conclusions obtained with each manipulation/procedure.

belonging to the Lachnospiraceae family were associated with reduced anxiety in exercised mice (Kang et al., 2014). Thus, enhancement in exercise might, indeed, contribute to the experience-dependent modifications observed in our microbiota data; however, other still unidentified cues coming from EE could work as commensal remodelers. Since the gut-brain axis is a bidirectional communication system, we cannot exclude that messages coming from the enriched brain may also shape the intestinal microbes in order to shift their metabolic potential toward specific biochemical pathways to sustain more dynamic and plastic neural circuitries.

Cellular underpinnings of gut microbiota action on ocular dominance plasticity

Strikingly, the depletion of the microbiota in EE mice completely blocked visual cortical plasticity. This effect was present both when animals were raised in EE from birth or only with a 5-week EE experience during adulthood. These experiments suggest that an intact microbiota contributes to the EE-dependent enhancement in cortical plasticity.

The microbiota depletion was performed using a classic approach consisting of the administration of a wide-spectrum antibiotic mix used in several gut-microbiota-brain axis studies (Chu et al., 2019; Desbonnet et al., 2015; Gacias et al., 2016; Olson et al., 2018). Furthermore, to exclude off-target effects of the antibiotic metronidazole on neural cells, we performed the same experimental protocol housing adult mice in EE for 5 weeks and administering metronidazole only. Metronidazole alone was not able to prevent the EE-driven enhancement in visual cortical plasticity. Instead, an ABX devoid of metronidazole blocked ocular dominance plasticity in EE mice, thus ruling out the possibility that plastic phenomena could be induced by a

direct influence of metronidazole on the brain, and indicating that synergistic alterations of the gut microbiota, rather than individual antimicrobial agents, are necessary to impinge on brain plasticity.

Importantly, microbiome depletion induced by 5-week ABX administration also affected two important EE-induced cellular mechanisms that have been previously involved in plasticity. Indeed, ABX-treated animals did not show increased dendritic spine dynamics and the microglial morphology typical of EE mice (Ali et al., 2019; Xu et al., 2016).

The intestinal microbiota has been shown to be a major determinant of microglia maturation, differentiation, and function (Erny et al., 2015). Microglia cells are essential players in neuropathology, although recent studies have highlighted their possible roles in brain physiology and plasticity (Wu et al., 2015). Various reports demonstrated that EE housing resulted in more numerous and longer microglial processes in different brain regions (Ali et al., 2019; Xu et al., 2016), demonstrating that microglia morphology in EE is more ramified with respect to standard conditions. Moreover, EE promotion of hippocampal neurogenesis is accompanied by microglia proliferation, and it is impaired in immune-deficient mice (Ziv et al., 2006). We found that ABX supplementation significantly impacted microglia morphology in the visual cortex, strongly decreasing its arborization and filament length. During the critical period, short MD makes microglial cells hyper-ramified, suggesting this shape-signature could be directly connected to ocular dominance plasticity (Sipe et al., 2016).

Notably, microglia has been suggested to phagocytose pre- and postsynaptic elements participating in synapse remodeling during development and plasticity (Cheadle et al., 2020; Hong et al., 2016; Paolicelli et al., 2011; Schafer et al., 2012; Schecter et al., 2017). Here, we observed that ABX-depletion of a functional microbiota not only impacted microglia morphology, but also dendritic spine dynamics in the visual cortex of adult EE rodents. Recent studies demonstrated that EE is able to increase dendritic spine dynamics in the cerebral cortex (Jung and Herms, 2014). Furthermore, spine remodeling has been shown to be a structural feature of plasticity in the visual system (Bochner et al., 2014; Chakravarthy et al., 2006; El-Boustani et al., 2018; Hofer et al., 2009; Mataga et al., 2004; Oray et al., 2004; Sajo et al., 2016; Sun et al., 2019; Vidal et al., 2016; Villa et al., 2016) and other sensory modalities (Holtmaat and Svoboda, 2009), suggesting that experience actively sculpts the synaptic landscape to modulate neural circuit function. Our data demonstrated that EE significantly enhanced spine density, through an increase in the growth of new spines. Remarkably, ABX administration counteracted EE-dependent structural plasticity in the visual cortex, as ABX inhibited the increase in spine density, while spine removal was virtually unaltered. Interfering with the microbiota in EE was essentially translated into hampering the biological processes underlying new spine formation. Our results are in line with previous work suggesting that the gut microbiota can modulate structural properties of the brain. In fact, germ-free mice show dendritic morphology and spine density alterations in various areas of the brain with positive or negative effects, depending on the brain area investigated (Luczynski et al., 2016, 2017). Importantly, our data were collected in adult animals in which the microbiota was depleted only in adulthood at the same time as EE, thus suggesting that paradigms that interfere with spine dynamics like EE, still rely on a healthy microbiome in adult age.

Searching a causal link between microbiota and cortical plasticity: SCFA administration and the fecal transplant

The gut microbiota could communicate with the brain influencing neural function through a variety of communication routes. Among them, our commensals contribute and complement host metabolism by modulating metabolic reactions and producing specific substrates such as SCFA. SCFAs act locally in the intestine and also participate in the maintenance of the host metabolic homeostasis by enhancing nutrient absorptions, and curbing the glycemic response (Alexander et al., 2019). Intriguingly, SCFAs can be released in the systemic circulation, cross the blood-brain-barrier, and reach the brain, where they have been demonstrated to be fundamental for blood-brain-barrier integrity (Braniste et al., 2014), microglia maturation, and homeostasis (Erny et al., 2015). Sodium butyrate decreases microglial activation, pro-inflammatory cytokine secretion (Patnala et al., 2017; Yamawaki et al., 2018), and promotes visual cortical plasticity (Silingardi et al., 2010). Also, acetate was recently shown to modulate microglial phagocytosis and disease progression during neurodegeneration (Erny et al., 2021). Interestingly, we found that living in EE increases the production of SCFAs. Furthermore, treating ST adult mice with oral SCFAs for 4 weeks mimicked the effects of fecal transplantation and EE, promoting ocular dominance plasticity. As SCFAs are highly versatile molecules, it is extremely difficult to envision a molecular mechanism for their effects on neural circuits, and the complexity and crosstalk among SCFA pathways acting on the brain further complicate the picture. SCFAs might affect microglia surveillance activity, and neural tissue epigenetic landscape, and thus gene expression, neurotransmitter levels, or SCFAs might act through indirect modulation of endocrine and immune pathways (Dalile et al., 2019). Here, we observed that SCFA treatment was associated with changes in microglia morphology in the visual cortex, rendering it hyper-ramified with respect to ST control. This shape has been observed in conditions of high plasticity, such as EE, and could favor ocular dominance plasticity through still unknown signals. Therefore, we are tempted to speculate that the microbiota could activate cortical plasticity mechanisms through SCFA-driven microglia remodeling. Future studies using metagenomic and metabolomic techniques will further dissect the bacteria-derived molecules involved, hopefully helping in the identification of specific mechanisms that could be targeted by new microbiota-based strategies for neurological diseases.

Transferring a specific phenotype by transplantation of the intestinal microbes is an important proof to causally link the microbiota to physiology and behavior. Strikingly, the transplantation of the fecal microbiota of EE mice to adult ST animals clearly induced ocular dominance plasticity. This is a key indication that the intestinal microbiota is involved in sensory system plasticity, a developmentally regulated process of plasticity. This observation suggests that EE-derived microbiota might be a powerful tool to trigger juvenile forms of plasticity, facilitating the recovery

from amblyopia or other serious conditions such as traumatic brain injury, stroke, and posttraumatic stress disorder, leading to alternative therapeutic strategies for neurodegenerative and neurodevelopmental diseases, or possibly enhancing cognitive performance in healthy subjects.

Also, our data prove that signals coming from the intestine overran the stability of the adult sensory circuits and the plasticity brakes.

In summary, these findings introduce a paramount concept: experience-dependent changes in the gut microbiota composition can modulate brain circuit function and plasticity. We propose the idea of an "experience-gut microbiota-brain" link: experience does not only impact the brain directly, but also through a pathway involving signals coming from the body periphery.

Limitations of the study

Although our study broadly assessed bacterial populations present in the different experimental condition mice using 16S rRNA-seq, this technique provides limited functional information about the microbiome. Future studies will explore this facet of the gut microbiota of EE mice utilizing shotgun metagenomic sequencing.

Another possible limitation of our study is related to sex-specific effects. In our work, both male and female mice were used, and we included sex as a variable in our statistical analyses; however, this reduced the number of analyzed mice. Thus, it could be that sex differences with relatively low effect size could be present. Thus, a deeper investigation with appropriate cohorts of male and female animals might unveil some distinct plasticity effects driven by the microbiota based on sex.

STAR★METHODS

Detailed methods are provided in the online version of this paper and include the following:

- KEY RESOURCES TABLE
- RESOURCE AVAILABILITY
  - Lead contact
  - Materials availability
  - Data and code availability
- EXPERIMENTAL MODEL AND SUBJECT DETAILS
  - Animals
- METHOD DETAILS
  - Antibiotic cocktail and short chain fatty acids administration
  - Faecal DNA extraction and 16S rRNA sequencing
  - SCFA quantification
  - Faecal transplantation
  - Monocular deprivation
  - Intrinsic optical signal imaging (IOS)
  - Two-photon imaging
  - Immunofluorescence analysis of microglial morphology
- QUANTIFICATION AND STATISTICAL ANALYSIS
  - Gut microbiota analysis
  - IOS experiments
  - Dendritic spines analysis
  - Microglia morphology

SUPPLEMENTAL INFORMATION

Supplemental information can be found online at https://doi.org/10.1016/j.celrep.2021.110212.

ACKNOWLEDGMENTS

We thank Francesca Damiani, Manuel Tongiani, Martina Nasisi, Matteo Caldarelli and Ornella Xynomilakis for their help with the experiments and Alexia Tiberi for help with Imaris Software. Special thanks to Vania Liverani and Antonella Calvello for technical assistance in the lab; Dr. Silvia Burchielli, Cecilia Ciampi, and Sara Ciampi for assistance in the vivarium; and Dr. Maria Cristina Casiraghi, Elisa Adele Colombo, and Giovanni Fiorillo for technical assistance for SCFA measurements. We thank Prof. Concetta Morrone and Prof. Paola Binda (University of Pisa) for their insightful comments. Two illustrations in the graphical abstract have been adapted from SciDraw (www.scidraw.io) under creative commons license (CC BY 4.0) (https://doi.org/10.5281/zenodo.4742583; https://doi.org/10.5281/zenodo.3925987).

This research was supported by H2020-MSCA-IF-2016 749697 GaMePLAY to P.T. and PRIN2017 2017HMH8FA to T.P.

AUTHOR CONTRIBUTIONS

L.L. and S.C. acquired, analyzed, and interpreted the data and critically revised the manuscript; G.S. acquired and analyzed the data; R.M. analyzed and interpreted the data; E.B., E.O., and M.D.C. performed the SCFA analysis and interpreted the data. P.T. performed the experiment and conceived the project. T.P. and P.T. wrote the manuscript and supervised the project.

DECLARATION OF INTERESTS

The authors declare no competing interests.

INCLUSION AND DIVERSITY

We worked to ensure sex balance in the selection of nonhuman subjects. One or more of the authors of this paper self-identifies as a member of the LGBTQ+ community. While citing references scientifically relevant for this work, we also actively worked to promote gender balance in our reference list.

Received: April 8, 2021
Revised: November 8, 2021
Accepted: December 14, 2021
Published: January 11, 2022

REFERENCES

Alexander, C., Swanson, K.S., Fahey, G.C., and Garleb, K.A. (2019). Perspective: physiologic importance of short-chain fatty acids from nondigestible carbohydrate fermentation. Adv. Nutr. *10*, 576–589.

Ali, S., Liu, X., Queen, N.J., Patel, R.S., Wilkins, R.K., Mo, X., and Cao, L. (2019). Long-term environmental enrichment affects microglial morphology in middle age mice. Aging *11*, 2388–2402.

Baroncelli, L., Braschi, C., Spolidoro, M., Begenisic, T., Sale, A., and Maffei, L. (2010). Nurturing brain plasticity: impact of environmental enrichment. Cell Death Differ. *17*, 1092–1103.

Baroncelli, L., Bonaccorsi, J., Milanese, M., Bonifacino, T., Giribaldi, F., Manno, I., Cenni, M.C., Berardi, N., Bonanno, G., Maffei, L., et al. (2012). Enriched experience and recovery from amblyopia in adult rats: impact of motor, social and sensory components. Neuropharmacology *62*, 2388–2397.

Bochner, D.N., Sapp, R.W., Adelson, J.D., Zhang, S., Lee, H., Djurisic, M., Syken, J., Dan, Y., and Shatz, C.J. (2014). Blocking PirB up-regulates spines

and functional synapses to unlock visual cortical plasticity and facilitate recovery from amblyopia. Sci. Transl. Med. *6*, 258ra140.

Boehme, M., Guzzetta, K.E., Bastiaanssen, T.F.S., van de Wouw, M., Moloney, G.M., Gual-Grau, A., Spichak, S., Olavarría-Ramírez, L., Fitzgerald, P., Morillas, E., et al. (2021). Microbiota from young mice counteracts selective age-associated behavioral deficits. Nat. Aging *1*, 666–676.

Borgo, F., Riva, A., Benetti, A., Casiraghi, M.C., Bertelli, S., Garbossa, S., Anselmetti, S., Scarone, S., Pontiroli, A.E., Morace, G., et al. (2017). Microbiota in anorexia nervosa: the triangle between bacterial species, metabolites and psychological tests. PLoS One *12*, e0179739.

Braniste, V., Al-Asmakh, M., Kowal, C., Anuar, F., Abbaspour, A., Tóth, M., Korecka, A., Bakocevic, N., Ng, L.G., Kundu, P., et al. (2014). The gut microbiota influences blood-brain barrier permeability in mice. Sci. Transl. Med. *6*, 263ra158.

Buffington, S.A., Di Prisco, G.V., Auchtung, T.A., Ajami, N.J., Petrosino, J.F., and Costa-Mattioli, M. (2016). Microbial reconstitution reverses maternal diet-induced social and synaptic deficits in offspring. Cell *165*, 1762–1775.

Buffington, S.A., Dooling, S.W., Sgritta, M., Noecker, C., Murillo, O.D., Felice, D.F., Turnbaugh, P.J., and Costa-Mattioli, M. (2021). Dissecting the contribution of host genetics and the microbiome in complex behaviors. Cell, 1740–1756.e16.

Callahan, B.J., McMurdie, P.J., Rosen, M.J., Han, A.W., Johnson, A.J.A., and Holmes, S.P. (2016). DADA2: high-resolution sample inference from Illumina amplicon data. Nat. Methods *13*, 581–583.

Cancedda, L., Putignano, E., Sale, A., Viegi, A., Berardi, N., and Maffei, L. (2004). Acceleration of visual system development by environmental enrichment. J. Neurosci. *24*, 4840–4848.

Cang, J., Kalatsky, V.A., Löwel, S., and Stryker, M.P. (2005). Optical imaging of the intrinsic signal as a measure of cortical plasticity in the mouse. Vis. Neurosci. *22*, 685–691.

Caporaso, J.G., Kuczynski, J., Stombaugh, J., Bittinger, K., Bushman, F.D., Costello, E.K., Fierer, N., Peña, A.G., Goodrich, J.K., Gordon, J.I., et al. (2010). QIIME allows analysis of high-throughput community sequencing data. Nat. Methods *7*, 335–336.

Chakravarthy, S., Saiepour, M.H., Bence, M., Perry, S., Hartman, R., Couey, J.J., Mansvelder, H.D., and Levelt, C.N. (2006). Postsynaptic TrkB signaling has distinct roles in spine maintenance in adult visual cortex and hippocampus. Proc. Natl. Acad. Sci. U. S. A. *103*, 1071–1076.

Champagne-Jorgensen, K., Kunze, W.A., Forsythe, P., Bienenstock, J., and McVey Neufeld, K.-A. (2019). Antibiotics and the nervous system: more than just the microbes? Brain Behav. Immun. *77*, 7–15.

Cheadle, L., Rivera, S.A., Phelps, J.S., Ennis, K.A., Stevens, B., Burkly, L.C., Lee, W.-C.A., and Greenberg, M.E. (2020). Sensory experience engages microglia to shape neural connectivity through a non-phagocytic mechanism. Neuron *108*, 451–468.e9.

Chu, C., Murdock, M.H., Jing, D., Won, T.H., Chung, H., Kressel, A.M., Tsaava, T., Addorisio, M.E., Putzel, G.G., Zhou, L., et al. (2019). The microbiota regulate neuronal function and fear extinction learning. Nature *574*, 543–548.

Cowan, C.S.M., Dinan, T.G., and Cryan, J.F. (2020). Annual Research Review: critical windows - the microbiota-gut-brain axis in neurocognitive development. J. Child. Psychol. Psychiatry *61*, 353–371.

Dalile, B., Van Oudenhove, L., Vervliet, B., and Verbeke, K. (2019). The role of short-chain fatty acids in microbiota-gut-brain communication. Nat. Rev. Gastroenterol. Hepatol. *16*, 461–478.

Darch, H.T., Collins, M.K., O'Riordan, K.J., and Cryan, J.F. (2021). Microbial memories: sex-dependent impact of the gut microbiome on hippocampal plasticity. Eur. J. Neurosci.

Desbonnet, L., Clarke, G., O'Sullivan, O., Cotter, P.D., Dinan, T.G., and Cryan, J.F. (2015). Re: gut microbiota depletion from early adolescence in mice: implications for brain and behaviour. Brain Behav. Immun. *50*, 335–336.

El-Boustani, S., Ip, J.P.K., Breton-Provencher, V., Knott, G.W., Okuno, H., Bito, H., and Sur, M. (2018). Locally coordinated synaptic plasticity of visual cortex neurons in vivo. Science *360*, 1349–1354.

Erny, D., Hrabě de Angelis, A.L., Jaitin, D., Wieghofer, P., Staszewski, O., David, E., Keren-Shaul, H., Mahlakoiv, T., Jakobshagen, K., Buch, T., et al. (2015). Host microbiota constantly control maturation and function of microglia in the CNS. Nat. Neurosci. *18*, 965–977.

Erny, D., Dokalis, N., Mezö, C., Castoldi, A., Mossad, O., Staszewski, O., Frosch, M., Villa, M., Fuchs, V., Mayer, A., et al. (2021). Microbiota-derived acetate enables the metabolic fitness of the brain innate immune system during health and disease. Cell Metab. *33*, 2260–2276.e7.

Evans, C.C., LePard, K.J., Kwak, J.W., Stancukas, M.C., Laskowski, S., Dougherty, J., Moulton, L., Glawe, A., Wang, Y., Leone, V., et al. (2014). Exercise prevents weight gain and alters the gut microbiota in a mouse model of high fat diet-induced obesity. PLoS One *9*, e92193.

Feng, G., Mellor, R.H., Bernstein, M., Keller-Peck, C., Nguyen, Q.T., Wallace, M., Nerbonne, J.M., Lichtman, J.W., and Sanes, J.R. (2000). Imaging neuronal subsets in transgenic mice expressing multiple spectral variants of GFP. Neuron *28*, 41–51.

Fischer, A., Sananbenesi, F., Wang, X., Dobbin, M., and Tsai, L.-H. (2007). Recovery of learning and memory is associated with chromatin remodelling. Nature *447*, 178–182.

Forsythe, P., and Bienenstock, J. (2016). Gut microbiota: microbiota and behaviour: visiting the sins of the mother. Nat. Rev. Gastroenterol. Hepatol. *13*, 502–504.

Gacias, M., Gaspari, S., Santos, P.-M.G., Tamburini, S., Andrade, M., Zhang, F., Shen, N., Tolstikov, V., Kiebish, M.A., Dupree, J.L., et al. (2016). Microbiota-driven transcriptional changes in prefrontal cortex override genetic differences in social behavior. Elife *5*.

Greifzu, F., Pielecka-Fortuna, J., Kalogeraki, E., Krempler, K., Favaro, P.D., Schlüter, O.M., and Löwel, S. (2014). Environmental enrichment extends ocular dominance plasticity into adulthood and protects from stroke-induced impairments of plasticity. Proc. Natl. Acad. Sci. U. S. A. *111*, 1150–1155.

Heimel, J.A., Hartman, R.J., Hermans, J.M., and Levelt, C.N. (2007). Screening mouse vision with intrinsic signal optical imaging. Eur. J. Neurosci. *25*, 795–804.

Hensch, T.K. (2005). Critical period plasticity in local cortical circuits. Nat. Rev. Neurosci. *6*, 877–888.

Higarza, S.G., Arboleya, S., Arias, J.L., Gueimonde, M., and Arias, N. (2021). Akkermansia muciniphila and environmental enrichment reverse cognitive impairment associated with high-fat high-cholesterol consumption in rats. Gut Microbes *13*, 1880240.

Hoban, A.E., Stilling, R.M., Ryan, F.J., Shanahan, F., Dinan, T.G., Claesson, M.J., Clarke, G., and Cryan, J.F. (2016). Regulation of prefrontal cortex myelination by the microbiota. Transl. Psychiatry *6*, e774.

Hofer, S.B., Mrsic-Flogel, T.D., Bonhoeffer, T., and Hübener, M. (2009). Experience leaves a lasting structural trace in cortical circuits. Nature *457*, 313–317.

Holtmaat, A., and Svoboda, K. (2009). Experience-dependent structural synaptic plasticity in the mammalian brain. Nat. Rev. Neurosci. *10*, 647–658.

Holtmaat, A., Bonhoeffer, T., Chow, D.K., Chuckowree, J., De Paola, V., Hofer, S.B., Hübener, M., Keck, T., Knott, G., Lee, W.-C.A., et al. (2009). Long-term, high-resolution imaging in the mouse neocortex through a chronic cranial window. Nat. Protoc. *4*, 1128–1144.

Holtmaat, A.J.G.D., Trachtenberg, J.T., Wilbrecht, L., Shepherd, G.M., Zhang, X., Knott, G.W., and Svoboda, K. (2005). Transient and persistent dendritic spines in the neocortex in vivo. Neuron *45*, 279–291.

Hong, S., Dissing-Olesen, L., and Stevens, B. (2016). New insights on the role of microglia in synaptic pruning in health and disease. Curr. Opin. Neurobiol. *36*, 128–134.

Hsiao, E.Y., McBride, S.W., Hsien, S., Sharon, G., Hyde, E.R., McCue, T., Codelli, J.A., Chow, J., Reisman, S.E., Petrosino, J.F., et al. (2013). Microbiota modulate behavioral and physiological abnormalities associated with neurodevelopmental disorders. Cell *155*, 1451–1463.

Hübener, M., and Bonhoeffer, T. (2014). Neuronal plasticity: beyond the critical period. Cell *159*, 727–737.

Jung, C.K.E., and Herms, J. (2014). Structural dynamics of dendritic spines are influenced by an environmental enrichment: an in vivo imaging study. Cereb. Cortex. *24*, 377–384.

Kang, S.S., Jeraldo, P.R., Kurti, A., Miller, M.E.B., Cook, M.D., Whitlock, K., Goldenfeld, N., Woods, J.A., White, B.A., Chia, N., et al. (2014). Diet and exercise orthogonally alter the gut microbiome and reveal independent associations with anxiety and cognition. Mol. Neurodegener. *9*, 36.

Kempermann, G. (2019). Environmental enrichment, new neurons and the neurobiology of individuality. Nat. Rev. Neurosci. *20*, 235–245.

Lehmann, K., and Löwel, S. (2008). Age-dependent ocular dominance plasticity in adult mice. PLoS One *3*, e3120.

Levelt, C.N., and Hübener, M. (2012). Critical-period plasticity in the visual cortex. Annu. Rev. Neurosci. *35*, 309–330.

Lozupone, C., and Knight, R. (2005). UniFrac: a new phylogenetic method for comparing microbial communities. Appl. Environ. Microbiol. *71*, 8228–8235.

Luczynski, P., Whelan, S.O., O'Sullivan, C., Clarke, G., Shanahan, F., Dinan, T.G., and Cryan, J.F. (2016). Adult microbiota-deficient mice have distinct dendritic morphological changes: differential effects in the amygdala and hippocampus. Eur. J. Neurosci. *44*, 2654–2666.

Luczynski, P., Tramullas, M., Viola, M., Shanahan, F., Clarke, G., O'Mahony, S., Dinan, T.G., and Cryan, J.F. (2017). Microbiota regulates visceral pain in the mouse. Elife *6, e25887*.

Mataga, N., Mizuguchi, Y., and Hensch, T.K. (2004). Experience-dependent pruning of dendritic spines in visual cortex by tissue plasminogen activator. Neuron *44*, 1031–1041.

Mazziotti, R., Lupori, L., Sagona, G., Gennaro, M., Della Sala, G., Putignano, E., and Pizzorusso, T. (2017). Searching for biomarkers of CDKL5 disorder: early-onset visual impairment in CDKL5 mutant mice. Hum. Mol. Genet. *26*, 2290–2298.

Mika, A., Van Treuren, W., González, A., Herrera, J.J., Knight, R., and Fleshner, M. (2015). Exercise is more effective at altering gut microbial composition and producing stable changes in lean mass in juvenile versus adult male F344 rats. PLoS One *10*, e0125889.

Möhle, L., Mattei, D., Heimesaat, M.M., Bereswill, S., Fischer, A., Alutis, M., French, T., Hambardzumyan, D., Matzinger, P., Dunay, I.R., et al. (2016). Ly6C(hi) monocytes provide a link between antibiotic-induced changes in gut microbiota and adult hippocampal neurogenesis. Cell Rep. *15*, 1945–1956.

Murakami, M., and Tognini, P. (2019). The circadian clock as an essential molecular link between host physiology and microorganisms. Front. Cell. Infect. Microbiol. *9*, 469.

Murakami, M., Tognini, P., Liu, Y., Eckel-Mahan, K.L., Baldi, P., and Sassone-Corsi, P. (2016). Gut microbiota directs PPAR γ-driven reprogramming of the liver circadian clock by nutritional challenge. EMBO Rep. *17*, 1292–1303.

Murmu, R.P., Li, W., Holtmaat, A., and Li, J.-Y. (2013). Dendritic spine instability leads to progressive neocortical spine loss in a mouse model of Huntington's disease. J. Neurosci. *33*, 12997–13009.

Nicholson, J.K., Holmes, E., Kinross, J., Burcelin, R., Gibson, G., Jia, W., and Pettersson, S. (2012). Host-gut microbiota metabolic interactions. Science *336*, 1262–1267.

Nithianantharajah, J., and Hannan, A.J. (2006). Enriched environments, experience-dependent plasticity and disorders of the nervous system. Nat. Rev. Neurosci. *7*, 697–709.

Nithianantharajah, J., Levis, H., and Murphy, M. (2004). Environmental enrichment results in cortical and subcortical changes in levels of synaptophysin and PSD-95 proteins. Neurobiol. Learn. Mem. *81*, 200–210.

Olson, C.A., Vuong, H.E., Yano, J.M., Liang, Q.Y., Nusbaum, D.J., and Hsiao, E.Y. (2018). The gut microbiota mediates the anti-seizure effects of the ketogenic diet. Cell *174*, 497.

Oray, S., Majewska, A., and Sur, M. (2004). Dendritic spine dynamics are regulated by monocular deprivation and extracellular matrix degradation. Neuron *44*, 1021–1030.

Paolicelli, R.C., Bolasco, G., Pagani, F., Maggi, L., Scianni, M., Panzanelli, P., Giustetto, M., Ferreira, T.A., Guiducci, E., Dumas, L., et al. (2011). Synaptic pruning by microglia is necessary for normal brain development. Science *333*, 1456–1458.

Patnala, R., Arumugam, T.V., Gupta, N., and Dheen, S.T. (2017). HDAC inhibitor sodium butyrate-mediated epigenetic regulation enhances neuroprotective function of microglia during ischemic stroke. Mol. Neurobiol. *54*, 6391–6411.

Pham, T.M., Winblad, B., Granholm, A.-C., and Mohammed, A.H. (2002). Environmental influences on brain neurotrophins in rats. Pharmacol. Biochem. Behav. *73*, 167–175.

Pizzorusso, T., Berardi, N., and Maffei, L. (2007). A richness that cures. Neuron *54*, 508–510.

van Praag, H., Kempermann, G., and Gage, F.H. (2000). Neural consequences of environmental enrichment. Nat. Rev. Neurosci. *1*, 191–198.

Rampon, C., Jiang, C.H., Dong, H., Tang, Y.P., Lockhart, D.J., Schultz, P.G., Tsien, J.Z., and Hu, Y. (2000). Effects of environmental enrichment on gene expression in the brain. Proc. Natl. Acad. Sci. U. S. A. *97*, 12880–12884.

Rooks, M.G., and Garrett, W.S. (2016). Gut microbiota, metabolites and host immunity. Nat. Rev. Immunol. *16*, 341–352.

Rosenzweig, M.R., and Bennett, E.L. (1996). Psychobiology of plasticity: effects of training and experience on brain and behavior. Behav. Brain Res. *78*, 57–65.

Sajo, M., Ellis-Davies, G., and Morishita, H. (2016). Lynx1 limits dendritic spine turnover in the adult visual cortex. J. Neurosci. *36*, 9472–9478.

Sale, A., Maya Vetencourt, J.F., Medini, P., Cenni, M.C., Baroncelli, L., De Pasquale, R., and Maffei, L. (2007). Environmental enrichment in adulthood promotes amblyopia recovery through a reduction of intracortical inhibition. Nat. Neurosci. *10*, 679–681.

Schafer, D.P., Lehrman, E.K., Kautzman, A.G., Koyama, R., Mardinly, A.R., Yamasaki, R., Ransohoff, R.M., Greenberg, M.E., Barres, B.A., and Stevens, B. (2012). Microglia sculpt postnatal neural circuits in an activity and complement-dependent manner. Neuron *74*, 691–705.

Schecter, R.W., Maher, E.E., Welsh, C.A., Stevens, B., Erisir, A., and Bear, M.F. (2017). Experience-dependent synaptic plasticity in V1 occurs without microglial CX3CR1. J. Neurosci. *37*, 10541–10553.

Schroeder, B.O., and Bäckhed, F. (2016). Signals from the gut microbiota to distant organs in physiology and disease. Nat. Med. *22*, 1079–1089.

Segata, N., Izard, J., Waldron, L., Gevers, D., Miropolsky, L., Garrett, W.S., and Huttenhower, C. (2011). Metagenomic biomarker discovery and explanation. Genome Biol. *12*, R60.

Silingardi, D., Scali, M., Belluomini, G., and Pizzorusso, T. (2010). Epigenetic treatments of adult rats promote recovery from visual acuity deficits induced by long-term monocular deprivation. Eur. J. Neurosci. *31*, 2185–2192.

Sipe, G.O., Lowery, R.L., Tremblay, M.-È., Kelly, E.A., Lamantia, C.E., and Majewska, A.K. (2016). Microglial P2Y12 is necessary for synaptic plasticity in mouse visual cortex. Nat. Commun. *7*, 10905.

Slaker, M., Barnes, J., Sorg, B.A., and Grimm, J.W. (2016). Impact of environmental enrichment on perineuronal nets in the prefrontal cortex following early and late abstinence from sucrose self-administration in rats. PLoS One *11*, e0168256.

Song, S.-Y., Chae, M., Yu, J.H., Lee, M.Y., Pyo, S., Shin, Y.-K., Baek, A., Park, J.-W., Park, E.S., Choi, J.Y., et al. (2018). Environmental enrichment upregulates striatal synaptic vesicle-associated proteins and improves motor function. Front. Neurol. *9*, 465.

Sun, Y.J., Espinosa, J.S., Hoseini, M.S., and Stryker, M.P. (2019). Experience-dependent structural plasticity at pre- and postsynaptic sites of layer 2/3 cells in developing visual cortex. Proc. Natl. Acad. Sci. U. S. A. *116*, 21812–21820.

Thukral, A.K. (2017). A review on measurement of Alpha diversity in biology. Agric. Res. J. *54*, 1.

Tognini, P. (2017). Gut microbiota: a potential regulator of neurodevelopment. Front. Cell Neurosci *11*, 25.

Tognini, P., Manno, I., Bonaccorsi, J., Cenni, M.C., Sale, A., and Maffei, L. (2012). Environmental enrichment promotes plasticity and visual acuity recovery in adult monocular amblyopic rats. PLoS One *7*, e34815.

Tremaroli, V., and Bäckhed, F. (2012). Functional interactions between the gut microbiota and host metabolism. Nature *489*, 242–249.

Vidal, G.S., Djurisic, M., Brown, K., Sapp, R.W., and Shatz, C.J. (2016). Cell-autonomous regulation of dendritic spine density by PirB. eNeuro *3*, 1–15.

Villa, K.L., Berry, K.P., Subramanian, J., Cha, J.W., Chan Oh, W., Kwon, H.-B., Kubota, Y., So, P.T.C., and Nedivi, E. (2016). Inhibitory synapses are repeatedly assembled and removed at persistent sites in vivo. Neuron *90*, 662–664.

Wang, B.-S., Feng, L., Liu, M., Liu, X., and Cang, J. (2013). Environmental enrichment rescues binocular matching of orientation preference in mice that have a precocious critical period. Neuron *80*, 198–209.

Wu, Y., Dissing-Olesen, L., MacVicar, B.A., and Stevens, B. (2015). Microglia: dynamic mediators of synapse development and plasticity. Trends Immunol. *36*, 605–613.

Xu, H., Gelyana, E., Rajsombath, M., Yang, T., Li, S., and Selkoe, D. (2016). Environmental enrichment potently prevents microglia-mediated neuroinflammation by human amyloid β-protein oligomers. J. Neurosci. *36*, 9041–9056.

Yamawaki, Y., Yoshioka, N., Nozaki, K., Ito, H., Oda, K., Harada, K., Shirawachi, S., Asano, S., Aizawa, H., Yamawaki, S., et al. (2018). Sodium butyrate abolishes lipopolysaccharide-induced depression-like behaviors and hippocampal microglial activation in mice. Brain Res. *1680*, 13–38.

Ziv, Y., Ron, N., Butovsky, O., Landa, G., Sudai, E., Greenberg, N., Cohen, H., Kipnis, J., and Schwartz, M. (2006). Immune cells contribute to the maintenance of neurogenesis and spatial learning abilities in adulthood. Nat. Neurosci. *9*, 268–275.

STAR★METHODS

KEY RESOURCES TABLE

REAGENT or RESOURCE	SOURCE	IDENTIFIER
Antibodies		
Anti-Iba-1	Wako	Cat. # 019-19741
Alexa Fluor 488–conjugated anti-rabbit secondary	Invitrogen	Cat. # A32731
Chemicals, peptides, and recombinant proteins		
Vancomycin hydrochloride	Duchefa Biochemie	Cat. # V0155.0005
Metronidazole	Sigma-Aldrich	Cat. # M3761
Ampicillin sodium salt	Sigma-Aldrich	Cat. # A9518
Neomycin sulfate	Gibco	Cat. # 1405-10-3
Sodium butyrate	Sigma-Aldrich	Cat. # 30341-0
Sodium propionate	Sigma-Aldrich	Cat. # P5436
Sodium Acetate	Sigma-Aldrich	Cat. # S8625
Critical commercial assays		
QIAamp Powerfecal DNA kit	Qiagen	Cat. # 12830-50
Deposited data		
16S rRNA-seq data	This study	Zenodo https://doi.org/10.5281/zenodo.5652187
Experimental models: Organisms/strains		
Mouse: C57BL/67	Jackson Laboratory	Stock No: 000664
Mouse: Thy1-GFP line M	Jackson Laboratory	Stock No: 007788
Software and algorithms		
GraphPad Prism version 7	GraphPad Software, San Diego, CA, USA	N/A
MATLAB software R_2017B	Mathworks	N/A
Imaris x64 software version 7.4.2	Bitplane	N/A
Python software 3.9.8	Python	N/A
MATLAB code for IOS Imaging experiment analysis	This study	Zenodo https://doi.org/10.5281/zenodo.5776770
MATLAB code for dendritic spine analysis	This study	Zenodo https://doi.org/10.5281/zenodo.5776563

RESOURCE AVAILABILITY

Lead contact

Further information and requests for resources and reagents should be directed to and will be fulfilled by the Lead Contact: Paola Tognini (paola.tognini@unipi.it).

Materials availability

This study did not generate new unique reagents.

Data and code availability

16S rRNA-seq data from P20, P25, P90 mice raised in ST or EE, and 16S rRNA-seq data from EE donor mice, ST recipient mice before and after fecal transplantation are publicly available at Zenodo: https://doi.org/10.5281/zenodo.5652187.

Custom MATLAB code for the analysis of IOS imaging experiments and for the measurement of ocular dominance index is publicly available at Zenodo: https://doi.org/10.5281/zenodo.5776770. Custom MATLAB code for the longitudinal analysis of dendritic spines is publicly available at Zenodo: https://doi.org/10.5281/zenodo.5776563.

Any additional information required to reanalyze the data reported in this paper is available from the lead contact upon request.

EXPERIMENTAL MODEL AND SUBJECT DETAILS

Animals

All experiments were carried out in accordance with the European Directives (2010/63/EU), and were approved by the Italian Ministry of Health (authorization number 140/2018-PR, 423/2021-PR).

Postnatal day (P)120 male and female C57BL/6J mice were used in this study, unless otherwise stated. ST mice were housed in conventional cages (365 x 207 x 140 mm, 2-3 animals per cage) with nesting material. Enriched mice were housed in larger cages (480 x 375 x 210 mm), in larger groups (5-6 mice per cage). Enriched cages were equipped with a variety of sterile toys of different shapes: running wheels, tunnels, tubes, climbing devices, triangle and igloos-shape shelter, food dispensers in different locations and nesting materials. The toys were substituted with new toys with different shapes and locations with respect to the previous week once a week, to ensure the novelty and continuous stimulation of the environment. The ST and EE cages used in all the experiments were individually ventilated cages to safely maintain the microbiota composition. Mice were housed in the same room, kept under a 12 hour dark: 12 hour light cycle, controlled temperature; and the same regimen of food (standard diet) and water administration ad libitum, was maintained for ST and EE.

METHOD DETAILS

Antibiotic cocktail and short chain fatty acids administration

A group of mice were raised in EE from birth. The dams of EE-pups were transferred from ST cages to EE cages 6-7 days before delivery. The large spectrum antibiotic cocktail (ABX, vancomycin 0.5 g/l, metronidazole 1 g/l, ampicillin 1 g/l and neomycin 1 g/l) was added to the dam's water when they were transferred in the EE cages. The litters continued to drink ABX after weaning (postnatal day (P) 21) until the day of ocular dominance plasticity assessment.

A second group of mice lived in EE only for 5 weeks during adulthood, from P85 to P120, and was exposed to the ABX in drinking water only during those 5 weeks. Other groups of mice living in EE for 5 weeks during adulthood also received an ABX without metronidazole (''ABX-metronidazole'' vancomycin 0.5 g/l, ampicillin 1 g/l and neomycin 1 g/l), or only metronidazole (1 g/l) in the drinking water.

To study dendritic spine dynamics, Thy-1 GFP transgenic mice (line M (Feng et al., 2000)) were housed in EE cages from P90 for 5 weeks. The control group had ad libitum access to water, while the treated group had ad libitum access to the ABX in drinking water for 5 weeks.

For all the experiments, the ABX was freshly prepared and changed every 2 days.

For the short chain fatty acids (SCFAs) treatment a mix of 25 mM sodium propionate, 40 mM sodium butyrate and 67.5 mM sodium acetate (Sigma-Aldrich) was added to drinking water as previously described (Erny et al., 2015) for 4 weeks from P90. The solution was freshly prepared and changed every 2 days. Regular water was administered to control mice.

To avoid cage-effects on our experiments, the animals used in all the experimental groups came from different EE or ST cages.

Faecal DNA extraction and 16S rRNA sequencing

To analyze the composition of the microbiota of ST and EE mice at different ages, fresh faeces were collected longitudinally in the same subject at P20, P25 and P90, snap-frozen in liquid nitrogen and stored at −80°C. To avoid the cage-effect on microbiota composition, the animals used for the analysis belonged to different cages and three different litters. Bacterial DNA was extracted using a specific kit (QIAamp Powerfecal DNA kit, Qiagen), and its concentration was quantified by Nanodrop 2000 C Spectrophotometer (ThermoFisher Scientific).

The 16S rRNA sequencing and analysis was performed by a service offered by Zymo Research (Irvine, CA, USA).

Targeted library preparation

The DNA samples were prepared for targeted sequencing with the Quick-16S™ NGS Library Prep Kit (Zymo Research). The primer sets used were Quick-16S™ Primer Set V3-V4 (Zymo Research). The sequencing library was prepared using an innovative library preparation process in which PCR reactions were performed in real-time PCR machines to control cycles and therefore limit PCR chimera formation. The final PCR products were quantified with qPCR fluorescence readings and pooled together based on equal molarity. The final pooled library was cleaned up with the Select-a-Size DNA Clean & Concentrator™, then quantified with TapeStation® (Agilent Technologies, Santa Clara, CA) and Qubit® (Thermo Fisher Scientific, Waltham, WA).

Control samples

The ZymoBIOMICS® Microbial Community Standard (Zymo Research) was used as a positive control for each DNA extraction, if performed. The ZymoBIOMICS® Microbial Community DNA Standard (Zymo Research) was used as a positive control for each targeted library preparation. Negative controls (i.e. blank extraction control, blank library preparation control) were included to assess the level of bioburden carried by the wet-lab process.

Sequencing

The final library was sequenced on Illumina® MiSeq™ with a v3 reagent kit (600 cycles). The sequencing was performed with >10% PhiX spike-in.

Bioinformatics analysis

Unique amplicon sequences were inferred from raw reads using the DADA2 pipeline (Callahan et al., 2016). Chimeric sequences were also removed with the DADA2 pipeline. Taxonomy assignment was performed using Uclust from Qiime v.1.9.1 with the Zymo Research Database, a 16S database that is internally designed and curated, as reference. Composition visualization, alpha-diversity, and beta-diversity analyses were performed with Qiime v.1.9.1 (Caporaso et al., 2010). If applicable, taxonomy that have significant abundance among different groups were identified by LEfSe using default settings (Segata et al., 2011).

SCFA quantification

Fecal short chain fatty acids (SCFAs) quantification was performed by GC-FID as previously described (Borgo et al., 2017). For each animal, 1 to 3 fecal pellets were collected and stored at −80°C until testing. Before the experiment, feces were weighted and suspended in double distilled water (1 mL), acidified with phosphoric acid (pH < 2) and extracted twice with diethyl ether-heptane (1:1 v/v). The aqueous phase was frozen at −80°C and the organic layer was collected for the analysis with a gas chromatography GC-2010 coupled to a flame ionization detector (FID) (Shimadzu, Kyoto, Japan). The GC was equipped with a Stabilwax-DA fused-silica capillary column (30 m, 0.53 mm i.d. with a film thickness 0.25 μm). The GC-FID conditions employed were: injection volume 1 μL, split ratio 3, helium flow rate 4.4 mL/min, injection temperature 200°C, and detector 250°C. The initial column temperature was 80°C and held 2 min, ramped to 250 at 8°C/min and kept at this temperature for 5 min with a total run time of 28 min. Quantification of the SCFAs was obtained through calibration curves of acetic, propionic, butyric, isobutyric, and isovaleric acids in concentrations between 0.15 and 5mM. Areas of the analytes were normalized by the response of 2-ethylbutyric acid, used as internal standard (IS).

SCFA concentrations ([SCFA]sample expressed as umol/mg) was obtained by applying the following formula:[SCFA] umol/mg = ($Area_{SCFA\ sample}$/$Area_{IS\ sample}$) x 1/($slope_{\ calibration\ curve}$) x 1000/mg feces

Faecal transplantation

Four different groups of adult (∼P120) EE C57BL/6J mice, living in different enrichment cages, or 4 different cages of age matched ST mice, were used as donors for this experiment. Recipient mice were adult C57BL/6J conventionally raised in ST condition, and housed 2/3 animals per cage. Before starting the faecal transplantation, the recipient mice were subjected to 1-week ABX in drinking water. After 2 days of washout, faecal transplantation was performed through oral gavage 5 times, once/day (Murakami et al., 2016). To avoid stress for the oral gavage, the procedure was performed for three consecutive days, the animals rested for 2 days, and finally were subjected to the gavage for another 2 days. At the time of faecal transplantation, freshly harvested EE or ST donor faeces were suspended in sterile PBS and mixed with a vortex for 10 min. The suspension was filtered with a cell strainer to remove large debris and immediately used for the transplantation. Every recipient mouse received 200 μl of suspension volume. A group of mice were orally gavaged with sterile PBS (the vehicle of the faeces suspension). After the inoculation, mice were left in their home cage to wait for the engraftment of new bacteria species for 4 weeks. Fresh faecal pellets from EE recipient mice were collected before the ABX treatment and 4 weeks after the transplantation. The animals analysed were housed in different cages to avoid the cage-effect on microbiota composition. DNA was extracted and 16S rRNA-seq was performed as explained in the previous section "Faecal DNA extraction and 16S rRNA sequencing".

Monocular deprivation

Mice were anesthetized with isoflurane (3% induction; 1% maintenance) and placed on a heated pad maintained at 37°C. The area surrounding the right eye was cleaned in a centrifugal manner with Povidone-iodine diluted 1:1 in saline using cotton swabs. The eye was covered with a thin layer of a dexamethasone/tobramycin ointment (Tobradex, Alcon Novartis) to prevent inflammation and infection. Eyelids were sutured with 3 or 4 horizontal mattress stitches by using a 6-0 surgical suture. After surgery, the animals were monitored and allowed to recover in a heated box.

Intrinsic optical signal imaging (IOS)

Surgery

Surgery for IOS imaging was performed as described in (Mazziotti et al., 2017). Mice were anesthetized with isoflurane (3% induction; 1% maintenance) and head fixed on a stereotaxic frame using ear bars. Body temperature was monitored using a heating pad and a rectal probe to maintain the animals' body at 37°C. A subcutaneous injection of lidocaine (2%) was provided to anesthetize the local area and the eyes were protected with a dexamethasone-based ointment (Tobradex, Alcon Novartis). The scalp was removed and the skull cleaned with saline. The skin was secured to the skull using cyanoacrylate and a thin layer of cyanoacrylate was poured over the exposed skull to attach a custom-made metal ring (9 mm internal diameter) centered over the binocular visual cortex. A thin layer of clear nail polish was applied over the area to ameliorate optical access. After surgery, the animals were allowed to recover fully in a heated box and monitored to ensure the absence of any sign of discomfort. Before any other experimental procedure, mice were left to recover for at least 48 hours.

Imaging and data analysis

Mice were anesthetized with isoflurane (3% induction; 1% maintenance) and chlorprothixene anesthesia (1.5 mg/kg, i.p.) at P120 and P123 (after 3 days of monocular deprivation) Images were visualized using a custom Leica microscope (Leica Microsystems). Red

light illumination was provided by 8 individually addressable LEDs (WS2812) attached to the objective (Leica Z6 APO coupled with a Leica PlanApo 2.0X 10447178) by a custom 3D-printed conical holder. Visual stimuli were generated using Matlab Psychtoolbox and presented on a gamma-corrected 24" monitor (C24F390FHU).

Horizontal sine-wave gratings were presented in the binocular portion of the visual field enclosed in a Gaussian envelope spanning -10 to +10 degrees of azimuth and -5 to +60 (full monitor height) degrees of altitude, with a spatial frequency of 0.03 cycles per degree, mean luminance 20 cd/m^2 and a contrast of 90%. The stimulus consisted of the abrupt contrast reversal of a grating with a temporal frequency of 4 Hz for 1 second, time-locked with a 12-bit depth acquisition camera (PCO edge 5.5) using a parallel port trigger. The interstimulus time was 13 seconds. Frames were acquired at 30 fps with a resolution of 540 x 640 pixels. The signal was averaged for at least 8 groups of 20 trials, stimulating each eye alternatively to prevent biases due to different time in anesthesia for the contralateral and ipsilateral eyes. The signal was then downsampled in time to 10 fps and in space to 270 x 320 pixels. Fluctuations of reflectance (R) for each pixel were computed as the normalized difference from the average baseline ($\Delta R/R$). For each recording, an image representing the mean evoked response was computed by averaging frames between 0.5 to 2.5 seconds after stimulation. The mean image was then low-pass filtered with a 2D average square spatial filter (7 pixels). To select the binocular portion of the primary visual cortex for further analysis, a region of interest (ROI) was automatically calculated on the mean image of the response of the ipsilateral eye by selecting the pixels in the lowest 30% $\Delta R/R$ of the range between the maximal and minimal intensity pixel (Cang et al., 2005). To weaken background fluctuations a manually selected polygonal region of reference (ROR) was subtracted. The ROR was placed where no clear response, blood vessel artifact or irregularities of the skull were observed (Heimel et al., 2007). Mean evoked responses were quantitatively estimated as the average intensity inside the ROI. To measure ocular dominance we used the Ocular Dominance Index (ODI) calculated as $ODI = \frac{C-I}{C+I}$ where C and I are the mean response amplitude evoked from contralateral and ipsilateral eye stimulation respectively. For the illustrations in the figures of the signal time course before and after MD, for each animal the contralateral and ipsilateral responses were normalized to the peak minimum value, and low-passed with a moving average (span: 3 samples). Signals were then averaged within each group.

Two-photon imaging

Surgery

Cranial windows were implanted on mice around P70. Animals were anesthetized with isoflurane (3% induction; 1% maintenance). Dexamethasone (subcutaneous 0.2 mg/kg) and Lidocaine (2%, 15-20 μL, subcutaneous, scalp area) were administered. After a few minutes, the scalp was cleaned with three swabs of povidone-iodine and a large portion of skin, covering both the hemispheres, was removed. The skull was cleaned from the periosteum by initially using saline and then by carefully scraping it with a scalpel blade. We drew a circular area of 3 mm of diameter centered 3 mm lateral, 1 mm anterior to lambda to mark the craniotomy area and we applied a thin layer of a light-curing dental cement on the rest of the exposed skull (3M Vitrebond™ plus). A metal head-plate was fixed to the skull by using more dental cement. By carefully using a dental drill and a biopsy punch, a 3 mm circular groove was thinned until almost transparent on the previously marked area, then a few drops of cold sterile ACSF were applied to the area. A circular island of bone was removed with the tip of a sharp forceps without damaging the dura. We placed and held in place a circular 3 mm coverslip on the craniotomy and secured it to the skull by using dental resin (Lang Contemporary Ortho Jet™). We then covered thoroughly the skull and the head-plate with more dental resin to finish the surgery. The animals were allowed to recover in a heated box and monitored to ensure the absence of any sign of discomfort. Before any other experimental procedure, mice were left to recover for 12-16 days to reduce inflammation in the surgical area, thus increasing the optical access to the tissue. A more detailed explanation for surgical procedures can be found in (Holtmaat et al., 2009)

Imaging and data analysis

Imaging was performed using a Bruker Ultima Investigator™ microscope equipped with a GaSsP Photomultiplier tube and controlled by the scanning software Prairie View. Laser excitation was provided by a tunable Ti:Sapphire pulsating LASER (Chameleon Ultra™, Coherent) tuned at 920 nm and excitation power was controlled with a Pockels Cell. LASER power was maintained under a maximum of 40 mW on the sample.

Images were acquired using a 20x long WD water immersion objective (Olympus XLUMPlanFL N 20x N.A. = 1.00). For each mouse, 1-3 pyramidal neurons with soma position in layer V were imaged. For each neuron, in the first session, we acquired an epifluorescence image of the vasculature of the imaging area to relocate the same dendritic segments on subsequent days. We then acquired a low-magnification two-photon stack of the entire apical dendritic arborization of the cell (1024x1024 pixels, x-y resolution: 0.46 μm/px, z step: 3 μm). 1-5 dendritic segments (imaging depth: 0-200 μm from the brain surface) per cell were chosen randomly between those that had better optical clarity, and a high-magnification stack of those segments was acquired (1024x1024 pixels, x-y resolution: 0.09 μm/px, z step: 1 μm). We ensured similar fluorescence across imaging sessions and, to prevent phototoxicity, the lowest laser power (< 40 mW) that could resolve all spines was used. Dendritic spines were counted manually with a custom-written MATLAB software by comparing simultaneously single, aligned z planes from the z-stacks of all 8 experimental time points. Images were first low-pass filtered with a 2D Gaussian filter (MATLAB function imgaussfilt, sigma: 1.1). We counted all clear spine protrusions emanating laterally from the dendrite, regardless of their shape (stubby, mushroom, thin). We considered the spines to be the same from one session to the other based on their relative position to structural landmarks and to very clear persistent spines present in all time points. Spines were considered different if they branched out from the dendritic segment more than 1 μm away from their previous position.

Spine Density was defined as the number of spines per μm of length of the dendritic segment. Similarly, the fraction of spines gained ($F_{(gained)}$) and lost ($F_{(lost)}$) between two time points t_1 and t_2 were defined as follows $F_{(gained)} = N_{(gain)}/N_{(t2)}*100$ and $F_{(lost)} = N_{(lost)}/N_{(t2)}*100$ (Holtmaat et al., 2005; Murmu et al., 2013). The time-dependent survival function was defined as $SF = N_{(t)}/N_{(0)}$ (Murmu et al., 2013) where $N_{(0)}$ is the number of spines present at the first imaging time point, and $N_{(t)}$ is the number of spines of the original set surviving after time t.

Immunofluorescence analysis of microglial morphology

Mice were anesthetized with chloral hydrate (20ml/Kg BW) and perfused via intracardiac infusion with PBS and then 4% paraformaldehyde (PFA, w/vol, dissolved in 0.1 M phosphate buffer, pH 7.4). Brains were quickly removed and post-fixed overnight in PFA at 4°C, then transferred to 30% sucrose (w/vol) solution. 45 μm coronal sections were cut on a freezing microtome (Leica) and free-floating sections were processed for immunofluorescence.

The cortical sections were incubated for 1 h in a blocking solution containing 5% BSA (w/vol) and 0.3% Triton X-100 (vol/vol) in PBS, and incubated overnight at 4°C with anti-Iba-1 (cat. no. 019-19741, Wako) diluted 1:500 in PBS with 1% BSA (w/vol) and 0.1% Triton X-100 (vol/vol).

Sections were then washed with PBS and incubated for 2h at 22-24°C with Alexa Fluor 488–conjugated secondary antibody (cat. no A32731, Invitrogen), which was added at a dilution of 1:500 in the same solution as the primary antibody.

Sections were washed three times with PBS and mounted on slides, then they were air-dried and coverslipped with Vectashield mounting medium (cat. H-1000,Vector Laboratories).

Imaging was performed on an LSM 900 confocal microscope (Zeiss, Oberkochen, Germany) using a Plan-Apochromat 63x, NA:1.4 oil objective.

The area of the visual cortex was defined based on the mouse brain atlas (Paxinos and Franklin's the Mouse Brain in Stereotaxic Coordinates).

Z-stacks of ~40 μm were acquired with a z-step of 0.50 μm (for a final voxel size of 0.1980717 × 0.1980717 × 0.5 μm). Images were then processed using the Filament Tracer Tool of IMARIS software (Bitplane). Between 5 and 10 cortical cells were reconstructed per analyzed mouse.

QUANTIFICATION AND STATISTICAL ANALYSIS

The sample sizes were based on prior studies and are indicated in the figure legend for each experiment. Whenever possible, quantification and analyses were performed blind to the experimental condition.

The majority of statistical analyses were performed using GraphPad Prism version 7 (GraphPad Software, San Diego, CA, USA).

Gut microbiota analysis

To test whether two or more groups of samples were significantly different, analysis of similarities (ANOSIM) and principal coordinate analysis were calculated using the Python library scikit-bio (http://scikit-bio.org/). The principal component analysis was performed on OTUs profiles using the Python package scikit-learn (https://scikit-learn.org/stable/).

IOS experiments

Differences between groups were tested for significance using two-way RM ANOVA, unless otherwise indicated. Holm–Sidak's multiple comparisons *post hoc* tests were performed, when appropriate, to correct for multiple hypothesis testing.

Dendritic spines analysis

Differences in spine density were evaluated using a two-way RM ANOVA time*housing. Holm–Sidak's multiple comparisons *post hoc* tests were performed, when appropriate, to correct for multiple hypothesis testing. Spine formation and elimination were compared with two-tailed t-test when comparing two housing groups, or with two-way RM ANOVA when comparing more than two groups.

Microglia morphology

For the analysis of filament length, number of branching points and dendrite terminals, statistical differences between groups were assessed using unpaired two-tailed Student's *t* test or Ordinary One-Way ANOVA followed by Tukey's *post hoc* multiple comparisons test. For the Sholl analysis, a Two-Way ANOVA was applied for main and interaction effects between distance from the soma and treatment, followed by Sidak's or Tukey's *post hoc* multiple comparisons test.

All data are represented as the mean ± SEM unless otherwise stated. N's represent single animals unless otherwise stated. Statistical significance was defined in the figure panels as follows: $*P < 0.05$, $**P < 0.01$ and $***P < 0.001$.